Catena 272 (2026) 110330

Contents lists available at ScienceDirect

Catena

journal homepage: www.elsevier.com/locate/catena

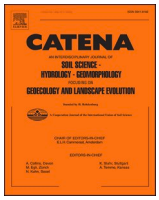

Late Holocene environmental dynamics and delta-lobe switching in the Razelm-Sinoe lagoon system, southern Danube delta (Romania)

Sabin Rotaru [a], Radu George Dimitriu [a], Dan Vasiliu [b], Bogdan Barbu [a], Bogdan Ispas [b], Andrei Briceag [a,*]

[a] National Institute of Marine Geology and Geo-ecology, GeoEcoMar, 23-25 Dimitrie Onciul Street, Bucharest, Romania
[b] National Institute of Marine Geology and Geo-ecology, GeoEcoMar, 304 Mamaia Blvd., Constanța, Romania

ARTICLE INFO

Keywords:
Ostracods
Lagoon
Multi-proxy analysis
Paleogeography
Black Sea
Geoarchaeology
Paleostorms

ABSTRACT

The Razelm-Sinoe lagoon system in the southern Danube Delta is a key archive for understanding how coastal environments respond to changing river, marine, and climate conditions. Although the region has been inhabited since the Neolithic, its environmental evolution during the Late Holocene is still not fully known. In this study, we reconstruct the past ~3000 years of lagoon history using a combination of sediment, geochemical, and fossil analyses. Our results show that the lagoon was strongly shaped by the shifting course of the Dunavăț distributary, which delivered large amounts of sediment and contributed to the formation of new delta lobes. High sedimentation rates (3.4 mm/year) around 2.6 ka BP indicate sustained river influence even in the outer parts of the lagoon. We identify five main stages of environmental change, from an open, river-dominated embayment to a progressively enclosed lagoon with occasional marine water intrusions, eventually leading to the development of widespread wetlands. By comparing paleosalinity signals from several cores, we detect four time intervals (~1.5–1.4, 1.3–1.2, 1.0–0.9, and 0.7–0.6 ka BP) when salinity increased across the system. These likely reflect periods of strong storms that breached coastal barriers and allowed seawater to enter the lagoon. We also explore how these changing conditions may have affected local settlements, offering new perspectives on how ancient communities adapted to a dynamic deltaic environment. Overall, this study provides an improved framework for understanding long-term coastal evolution and environmental variability in the Danube Delta.

1. Introduction

Coastal lagoons are dynamic, shallow, and semi-enclosed transitional environments shaped by the interplay of marine, fluvial, and climatic forcing (Duck and Da Silva, 2012). Their limited depth enhances their sensitivity to variations in relative sea level, freshwater inflow, and storm activity, making them valuable natural archives for detecting environmental change across multiple timescales (Sabatier et al., 2010; Chaumillon et al., 2017).

Coastal lagoons and deltaic systems have long attracted human societies due to their ecological productivity, strategic location, and access to both marine and terrestrial resources. In the Mediterranean and Black Sea regions, these environments have mediated not only the location and structure of human settlements but also their long-term sustainability and evolution (Morhange et al., 2016; Giaime et al., 2019). The western Black Sea coast supported numerous communities whose development was strongly influenced by evolving lagoonal and deltaic conditions. Greek colonization between the 8th and 5th centuries BCE resulted in the establishment of settlements such as Histria, Orgame, and Halmyris along the Danube delta coast (Bivolaru et al., 2021; Dimitriu, 2012). Understanding paleoenvironmental dynamics is therefore essential not only for reconstructing the evolution of the Razelm-Sinoe Lagoon System (RSLS) but also for contextualizing ancient settlement patterns and cultural adaptations in this region.

Compared with Mediterranean lagoons, the Holocene evolution of Black Sea lagoons remains relatively understudied, particularly regarding sedimentation history, hydrological variability, and responses to extreme events. For RSLS, previous work has focused primarily on barrier morphodynamics and southern Danube delta progradation (Zenkovich, 1956; Giosan et al., 2006; Vespremeanu-Stroe et al., 2013, 2017), while the internal lagoonal environment – its sedimentation rates, ecosystem history, and hydrological evolution – remains poorly constrained. This limits understanding of the lagoon's connection to the Dunavăț distributary, specifically regarding the mechanism of the RSLS's

* Corresponding author.
E-mail address: andrei.briceag@geoecomar.ro (A. Briceag).

https://doi.org/10.1016/j.catena.2026.110330
Received 20 June 2025; Received in revised form 5 June 2026; Accepted 8 June 2026
Available online 20 June 2026

final enclosure, around which a longstanding scientific debate persists. Two competing models propose either (i) southward longshore sediment transport leading to RSLS enclosure, implying that Dunavăț remained a bayhead lobe (Zenkovich, 1956; Giosan et al., 2006; Bony et al., 2015), or (ii) progradation and reworking of two successive open-sea lobes built by the Dunavăț branch (Antipa, 1914; Panin, 1989; Vespremeanu-Stroe et al., 2013, 2017).

This study employs ostracods, which are valuable microfossils due to their high sensitivity to salinity, oxygen levels, and hydrological changes (Holmes and De Deckker, 2012; Marco-Barba et al., 2013). Their species composition and relative abundances effectively trace environmental variability in transitional settings like lagoons. Beyond their established paleoecological utility, ostracods are increasingly recognized as powerful tools for identifying paleostorm events in barrier-lagoon systems (Mischke et al., 2012; Sabatier et al., 2022). For the Black Sea region, where paleostorm research is virtually absent, applying ostracods for storm reconstruction represents a methodological advancement with broader implications for coastal paleoclimate studies.

This work addresses critical gaps in the understanding of RSLS's Late Holocene evolution by examining sedimentary dynamics, paleoecological changes, and evidence for extreme events. It constitutes the first integrated multi-proxy reconstruction of the Late Holocene history of the Razelm-Sinoe system, combining sedimentological, geochemical, and faunal analyses. The newly recovered core F1, obtained from a key geoarchaeological site, provides a high-resolution archive that links environmental change with cultural developments and fills a spatial and temporal gap in existing reconstructions. Comparison with other RSLS records further allows a regional synthesis of sedimentation rates and environmental trajectories.

This study was conducted to clarify how natural and human factors shaped the Late Holocene evolution of the Razelm-Sinoe lagoon complex. It addresses three interconnected themes. First, we reconstruct landscape transformations and paleoecological evolution over the last ~3000 years, identifying shifts in sedimentation, salinity, and faunal assemblages. High-resolution sampling enables the recognition of five lagoonal evolutionary phases, revealing transitions not captured in previous studies. Second, we analyze biotic and sedimentary indicators of environmental change, including the innovative use of ostracods to infer past storm events, thereby establishing the first paleostorm framework for the Black Sea. Third, we examine human – environment interactions by linking lagoonal evolution with nearby archaeological sites – Histria, Orgame, and Acic Suat – offering new perspectives on landscape evolution and cultural adaptation in a deltaic context. Together, these analyses provide novel insights into sedimentary processes, environmental variability, and societal responses to coastal change, with broader implications for regional paleoclimate reconstruction and coastal management in the Black Sea.

2. Study area

2.1. Regional setting

The study area is located in the western part of the Razelm-Sinoe Lagoon System (RSLS), representing a marshy plain separating Ceamurlia and Golovița lakes (Fig. 1). The RSLS covers 1145 km^2 and comprises shallow lakes and lagoons (maximum depth - 3.5 m in Razelm), wetlands, channels, barrier complexes, and beach ridge plains, forming the southern Danube Delta. Freshwater inflow comes primarily from the Danube River (discharge of ~6500 m^3/s at the delta apex) via the Dunavăț and Dranov channels, with smaller contributions from rivers draining the Dobrogea mainland, including the nearby Slava and Hamangia. Although these smaller rivers have low mean annual discharge (< 0.7 m^3/s), flash floods can produce peak discharges of 100 – > 400 m^3/s during summer (Zaharia and Pisota, 2003). The RSLS is connected to the Black Sea only in the southern sector via Lake Sinoe and its narrow outlets at Edighiol and Periboina.

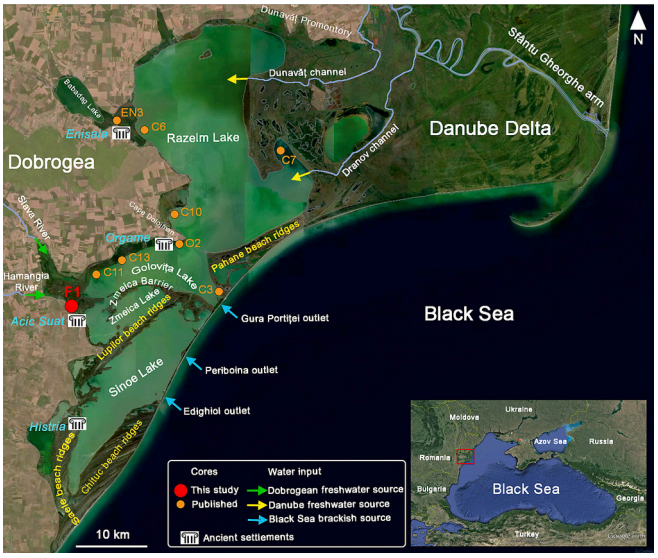

Fig. 1. Location of the study area and the core F1 (red circle) on a Copernicus Landsat image in the background, and the main toponyms and hydronyms which are referred to in the text. Published cores are from Preoteasa et al., 2019 (EN3), van de Velde et al., 2019 (C3 – C13), and Bony et al., 2015 (O2). (For interpretation of the references to color in this figure legend, the reader is referred to the web version of this article.)

Present-day salinity ranges from 0.4 to 0.6 g/L in Razelm and Golovița and 0.5–6.5 g/L in Sinoe, while historical values in the early 20th century reached up to 27.8 g/L (Vadineanu et al., 1997). Salinity is seasonally controlled by freshwater input from Danube high discharges during April–May and September–October (Scrieciu et al., 2023a), and by storm-driven mesohaline inflows during October–March (Catianis et al., 2018). 80% of the total storm events (including extreme storms) are from a N-NE direction influencing the current shoreline orientation and morphodynamics, and generating a strong southward net longshore sediment transport of 0.7–1 × 10^6 m^3/year which can quadruple during storms (Dan et al., 2009; Zăinescu et al., 2017). Severe storms recur every 0.5–2 years, while extreme storms recur roughly every 7 years, with wind speeds exceeding 30 m/s and offshore waves up to 7 m, causing severe coastal erosion and extensive flooding (Vespremeanu-Stroe, 2004; Zăinescu et al., 2017).

Geologically, the study area lies at the contact between the Paleozoic Moesian Platform in the south and the Cimmerian Orogen of North Dobrogea in the north, separated by the Peceanaga-Camena fault (Săndulescu, 1984). The Moesian Platform comprises a Precambrian basement overlain by thick Paleozoic to Cenozoic sediments, while the Cimmerian Orogen consists of a Hercynian basement with post-tectonic cover of Upper Cretaceous shallow-marine sediments (Seghedi, 2012). Thick Quaternary loess deposits cover much of the Dobrogea territory (Conea, 1970).

2.2. Geoarchaeological context

Acic-Suat is located between the Greek colonies of Histria and Orgame and was occupied from the 6th century BCE through the early Roman period. The settlement had a subsistence-based economy focused on cereal cultivation, livestock, and freshwater fishing, while archaeological evidence indicates both Greek and local influences (Baralis et al., 2017; Musat, 2017). Its strategic position between Lakes Golovița and Sinoe provided access to inland and maritime networks, linking it to Histria and other regional centers. During the Roman period, the site underwent spatial reorganization, reflecting integration into provincial structures and connections with nearby colonial settlements (Baralis et al., 2017).

3. Material and methods

Core F1 was retrieved using a percussion corer system (Atlas Copco Cobra TT) from the Ceamurlia Lake, located on the western bank of the Razelm-Sinoe lagoon complex (44°40′28.70“ N, 28°45’7.34” S). The 7 m sediment core was sampled for sedimentological, geochemical and paleontological (micro and macro) analyses as well as for radiocarbon dating. Sampling resolution (10–30 cm) was adjusted according to lithology, sediment preservation, and available core volume. Higher-resolution sampling was prioritised in intervals with high information potential (e.g., transitions, biogenic layers), whereas massive or low-variability units were sampled at coarser resolution.

Prior to sampling the core for laboratory analyses, magnetic susceptibility was measured at 1 cm intervals using a Bartington MS2C system. The sensor used has a response area with a diameter of 25.4 mm.

Grain-size samples were collected at an average interval of 30 cm, with increased sampling density in areas showing visible changes in texture. Prior to analysis, the samples were treated with 20% acetic acid (CH_3COOH) and 30% hydrogen peroxide (H_2O_2) to eliminate organic matter, followed by rinsing with distilled water. Measurements were performed using a Horiba LA950 Laser Diffraction Particle Size Analyzer. Statistical analysis of the grain-size data was conducted with the GRADISTATv8 software (Blott and Pye, 2001), employing the Folk and Ward (1957) method.

Organic matter (OM) and inorganic carbonate (C_{inorg}) content were determined through Loss on Ignition (LOI) analysis. Samples were taken at approximately 15 cm intervals and placed in crucibles for sequential combustion in a Caloris CD 1011 oven: first at 105 °C for 12 h, then at 550 °C for 6 h, and finally at 950 °C for 2 h, with precise weighing after each step. The percentages of OM and C_{inorg} were calculated using the equations provided by Heiri et al. (2001).

Major, minor and trace components in surficial sediment samples were analyzed by X-ray fluorescence spectrometry using an ED-XRF SPECTRO XEPOS spectrometer (SPECTRO Analytical Instruments GmbH, Kleve, Germany). Major and minor components measured as percentage oxides were converted to ppm levels. Potential diagenetic overprinting was considered when evaluating geochemical data. Organic-rich and oxidized intervals may have experienced post-depositional alteration, which can modify elemental concentrations and further affect the preservation of calcareous microfossils. These factors may limit the precision of source discrimination and paleoenvironmental reconstructions.

Principal component analysis (PCA) was used to statistically determine the main changes in geochemical elements using a correlation matrix of all the elements contents. The geochemical dataset consisted of eighteen elemental contents which were transformed into a standardized and mean normalized distribution. To evaluate sediment provenance, the PCA was repeated by integrating reference datasets representing the main regional sources: Danube riverbed (Scrieciu et al., 2023b), Dobrogea loess (Tugulan et al., 2016), granites (Întorsureanu et al., 1989), and rhyolites (Seghedi et al., 1992) (Table 1). All datasets were processed using the same normalization steps to ensure comparability. The major shifts in the first two PC axes in the sample scores were used to divide the elements into ultimately two major sediment sources. Sample and element relationships were further explored using hierarchical clustering to evidence the contribution of each element in the geochemistry of the sediment sources. These statistical analyses were performed using the SRplot online tool (Tang et al., 2023).

Micro- and macrofaunal analyses were carried out on samples retrieved on an average 10 cm resolution, to infer water paleosalinity and depositional environments. The samples were processed for microfossil analyses using a standard micropaleontological approach (Stoica et al., 2013; Briceag et al., 2019). Samples were oven dried at 60 °C, weighed and then wet-sieved using tap water and sieves of 125 μm and 63 μm. All valves larger than 125 μm belonging to ostracods and bivalves were observed and qualitatively estimated, as well as all foraminifera and gastropod individual specimens. Qualitative abundances were obtained by estimating the specimens within the field of view. Large specimen occurrences are considered to be more than 100 individuals, moderate occurrences – between 10 and 30 individuals, while less than 10 valves indicate a scarce presence. Species identification and paleoecological interpretation followed established taxonomic works: Caraion (1967), Meisch (2000), and Opreanu (2008) for ostracods; Kaminski et al. (2002) and Briceag and Ion (2014) for foraminifers; and Grossu (1955, 1956) for mollusks. Ostracod paleoecological assignments were based on Meisch (2000) for freshwater taxa and on Caraion (1967) and Opreanu (2008) for brackish and marine species. The subdivision of ostracod ecological groups follows the criteria outlined in Mazzini et al. (2022). Ostracods provide robust salinity signals and form the main basis of our interpretations, with other proxies as foraminifers and mollusks used as supplementary context. However, short-term hydrological or climatic variability may not be fully captured. The most representative fauna was documented by photographs made with a Canon EOS 550D camera mounted on a binocular microscope Olympus SZ61 (Plates 1 and 2).

The chronological framework of core F1 is based on four calibrated radiocarbon dates obtained from ostracod valves, primarily *Cyprideis torosa* (Table 2). The ^{14}C AMS measurements were carried out at the Poznań Radiocarbon Laboratory in Poland. Calibration of the radiocarbon ages was performed using the Marine20 calibration curve (Heaton et al., 2020) in Oxcal 4.4 program (Bronk Ramsey, 2001). The marine calibration accounts for the average global ocean reservoir effect, which is ~400 years. To account for local conditions, a regional ΔR value of 75 ± 65, derived from Siani et al. (2000), was applied. This estimate is based on surficial Black Sea waters and is the most appropriate for the shallow lagoonal environment of core F1. The use of Siani's ΔR is also consistent with previous chronological studies in the Danube Delta region (Bony et al., 2015; Vespremeanu-Stroe et al., 2017) and provides a robust framework for our radiocarbon chronology.

4. Results

4.1. Sediment properties and geochemical analysis

Core F1 was divided in three main units based on geochemical composition of the sediments, grain size and texture, organic matter content and magnetic susceptibility properties (Fig. 2).

Core F1 is predominantly composed of fine to medium silts with layers of sandy silts and frequent occurrences of shell and plant

Table 1
The average content (ppm) of main elements of the regional sediment sources: Danube riverbed (Scrieciu et al., 2023b), Dobrogea loess (Tugulan et al., 2016), Dobrogea granites (Întorsureanu et al., 1989), and Dobrogea rhyolites (Seghedi et al., 1992).

Sediment source samples	Elements (ppm)														
	Ti	Fe	V	Mg	Mn	K	Rb	Zr	Si	Th	Sn	Cr	Ni	Sr	Ca
Danube	2369.2	20,130.7	40.5	14,783.6	486.0	12,808.7	55.3	140.7	247,106.7	3.7	3.1	75.1	42.3	182.0	53,914.7
Rhyolites	1238.8	14,221.1	4.3	1236.8	293.7	36,428.1	96.3	406.3	355,228.3	13.9	4.1	2.1	2.8	17.4	3377.7
Granites	1474.6	15,170.0	1.5	1338.9	873.5	38,774.0	140.3	636.5	345,519.9	18.6	5.7	5.0	4.5	18.4	4409.1
Loess	4190.0	37,375.9	92.4	14,944.8	749.8	16,519.0	88.0	461.4	293,706.9	11.5	4.3	121.8	58.5	255.9	67,979.9

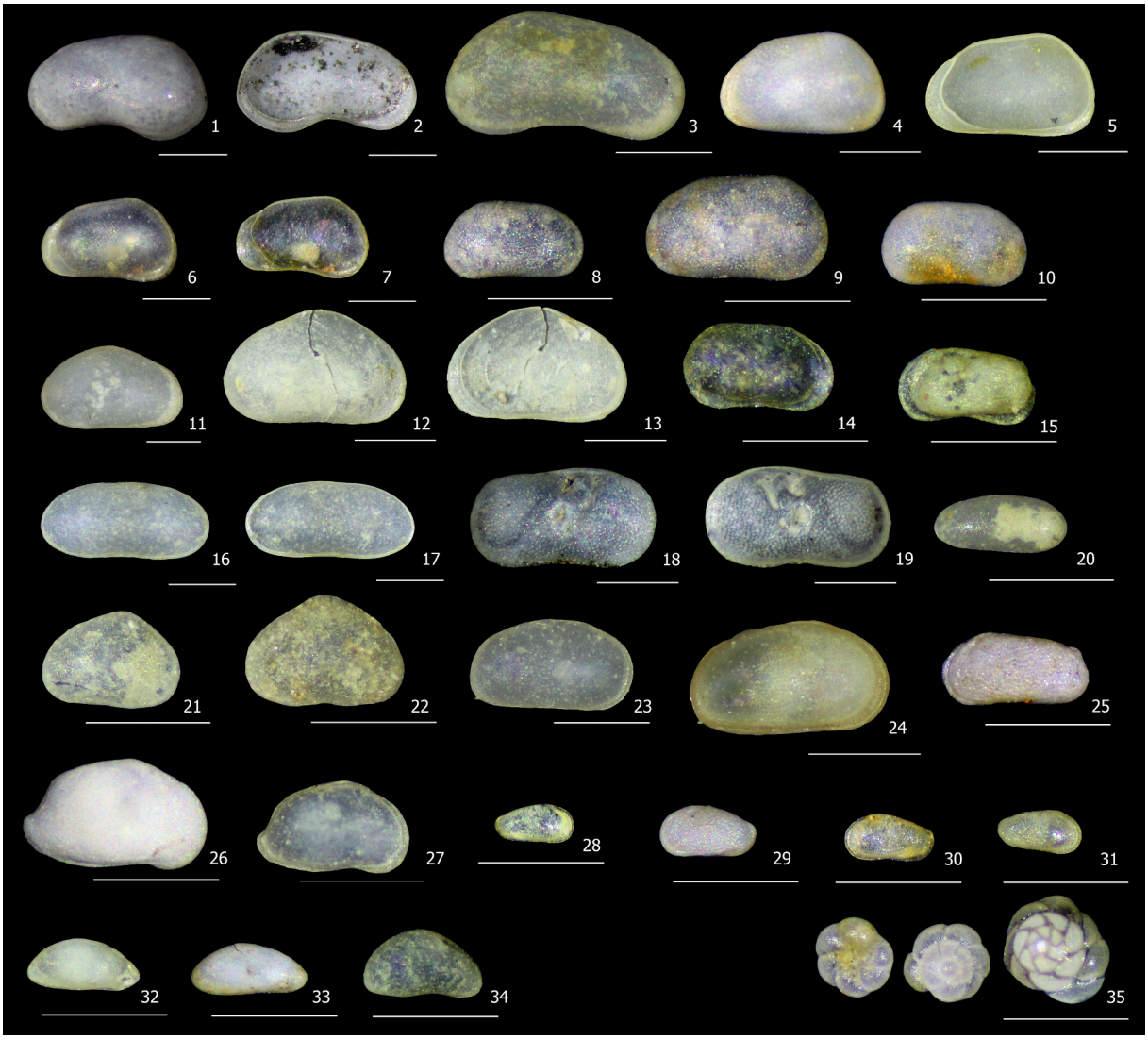

Plate 1. Microfaunal assemblages from F1 core. The ostracods are photographed in external lateral view except 2, 5, 7 and 13 that are photographed in internal lateral view. All scales represent 0.5 mm. Ostracods: 1–3 – *Candona neglecta*; 4–7 – *Pseudocandona compressa*; 8 – *Pseudocandona albicans*; 9–10 – *Pseudocandona* sp.; 11–13 – *Heterocypris salina*; 14–15 – *Limnocythere inopinata*; 16–17 – *Herpetocypris reptans*; 18–19 – *Ilyocypris bradyi*; 20 – *Darwinula stevensoni*; 21–22 – *Eucypris inflata*; 23–24 – *Cyprideis torosa*; 25 – *Cytheromorpha fuscata*; 26–27 – *Heterocythereis amnicola*; 28 – *Amnicythere pediformis*; 29–31 – *Amnicythere devexa*; 32–33 – *Cytherois cepa*; 34 – *Xestoleberis aurantia*; Foraminifers: 35 – *Ammonia* spp.

fragments. Sediment sorting is relatively consistent, varying between very poorly and poorly sorted sediments. Organic matter content shows moderate variability, peaking in the upper section of the core. In contrast, magnetic susceptibility and geochemical data exhibit the highest variability. A sediment loss occurred during coring between 380 and 460 cm, but field observations indicate that the missing interval is lithologically similar to the adjacent sections.

4.1.1. Unit 1 (705–325 cm)

This unit consists of mainly fine, semi-compact, very poorly sorted silts (40%) with very few plants remains. Clays, coarse silts and fine sands are on average 20, 25 and 10% respectively. Organic matter (OM) content is consistently low (3,5%). The magnetic susceptibility (MS) values are fairly high with a mean of 2.85×10^{-6} CGS (Fig. 2). Terrigenous elements display elevated mean concentrations: Zr (400 ppm), Mg (17,000 ppm), Ti (4400 ppm), Fe (2800 ppm), and Cr (96 ppm), accompanied by high Ca values (58,000 ppm). The increased terrigenous values are in contrast with the low OM and Sulfur contents, reflected also in the high Si/S ratio.

We divided Unit 1 into two subunits (1a and 1b) based on changes sediment color and magnetic susceptibility properties at 555 cm core depth. Subunit 1a consists of reddish-brown silts, whereas Subunit 1b is characterized by dark grey silts with thin purplish layers and intercalations of yellowish-brown silts. The MS mean values drop by half, from 3.8×10^{-6} CGS in subunit 1a to 2×10^{-6} CGS in subunit 1b (Fig. 2).

4.1.2. Unit 2 (325–185 cm)

The 330 cm boundary marks changes in all sediment properties (Fig. 2). Unit 2 is coarser than Unit 1 with increased coarse silts (30%) and sands (17%). The coarsening is also evident in the lowest mean Al/Si values (0.19) of the entire core. The lower half of the unit contains grey coarse silts, gradually finning upwards into blackish medium silts with brown colored laminae. Sorting is poor, however slightly better than in the previous unit. OM content triples compared with the lower units reaching its highest mean values (12%), with maximal peaks of 15–25% toward the top of the interval. S concentrations also reach their highest values (> 6000 ppm). MS continues its downward trend, reaching the lowest average value of 0.8×10^{-6} CGS. Most of the terrigenous content declines, with elements such as K (14,000 ppm), Rb (65 ppm), Ti (3600

Plate 2. Macrofaunal assemblages from F1 core: A – *Abra segmentum*; B and D – *Ecrobia* sp.; C – *Planorbarius corneus*; E – *Parthenina terebellum*; F – *Charophyceae* algae; G and H – *Cerastoderma* sp.; I - *Theodoxus danubialis*. All scales represent 0.5 mm.

Table 2
Summary of radiocarbon age results.

Sample	Lab code	Depth in core (cm)	Material	Coordinates (lat. N/long. S)	Age ^{14}C (years BP)	Cal. Age BP (2σ)	Median Age (cal. yr BP)
F1 AS 130	Poz-151,421	130	Ostracods	44°40′28.70″/ 28°45′7.34”	1515 ± 30	656–1023	863
F1 AS 225	Poz-144,596	225	Ostracods	44°40′28.70″/ 28°45′7.34”	2020 ± 30	1170–1531	1353
F1 AS 250	Poz-151,423	250	Ostracods	44°40′28.70″/ 28°45′7.34”	2250 ± 30	1392–1807	1590
F1 AS 550	Poz-151,392	550	Ostracods	44°40′28.70″/ 28°45′7.34”	2975 ± 30	2298–2719	2493

ppm), Mn (500 pm) and Fe (21,000 ppm) recording their lowest mean values. Conversely, elements such as Ca (6200 ppm), S (4500 ppm), Sr (282 ppm) registered their highest mean values of the entire core. Si (265,000 ppm) and P (470 ppm) indicate as well increased values.

4.1.3. Unit 3 (185–0 cm)

Unit 3 is composed of very fine to fine brown silts with purplish laminae, with a central layer of coarse silts and capped by a peat deposit. In the middle part of the unit there is a section of purplish-grey color (Fig. 2). Clay content increased significantly (23%), while sand content halved (8%) and coarse silts decreased (23%) compared with Unit 2. Unit 3 starts with an abrupt decrease in mean OM content (down to 5.5%) and S (1500 ppm). MS increases sharply and records the highest mean values of the core (4.1×10^{-6} CGS). Unit 3 samples are mainly clustered in relation to PC_1 indicating negative loads in relation to PC_2. They are generally grouped based on contents in Si, P, Rb, K, Mn and secondarily on Ni, Fe, Zn, Al (Fig. 3A and B).

Unit 3 was divided into Subunits 3a and 3b based on a decreasing trend in multiple geochemical elements toward the top of the core. Subunit 3a contains the highest mean concentrations of several terrigenous elements in the entire core – K (18,500 ppm), Fe (31,000 ppm), Mn (720 ppm), Ti (4600 ppm), Rb (90 ppm), Cr (99 ppm), Ni (47 ppm). In Subunit 3b these values decrease to Mn (670 ppm), Fe (28,000 ppm), Rb (78 ppm), Ti (4300 ppm), Cr (82 ppm) and Ni (37 ppm). Si increases upward, consistent with higher silt percentages (28% vs. 18% in subunit 3a).

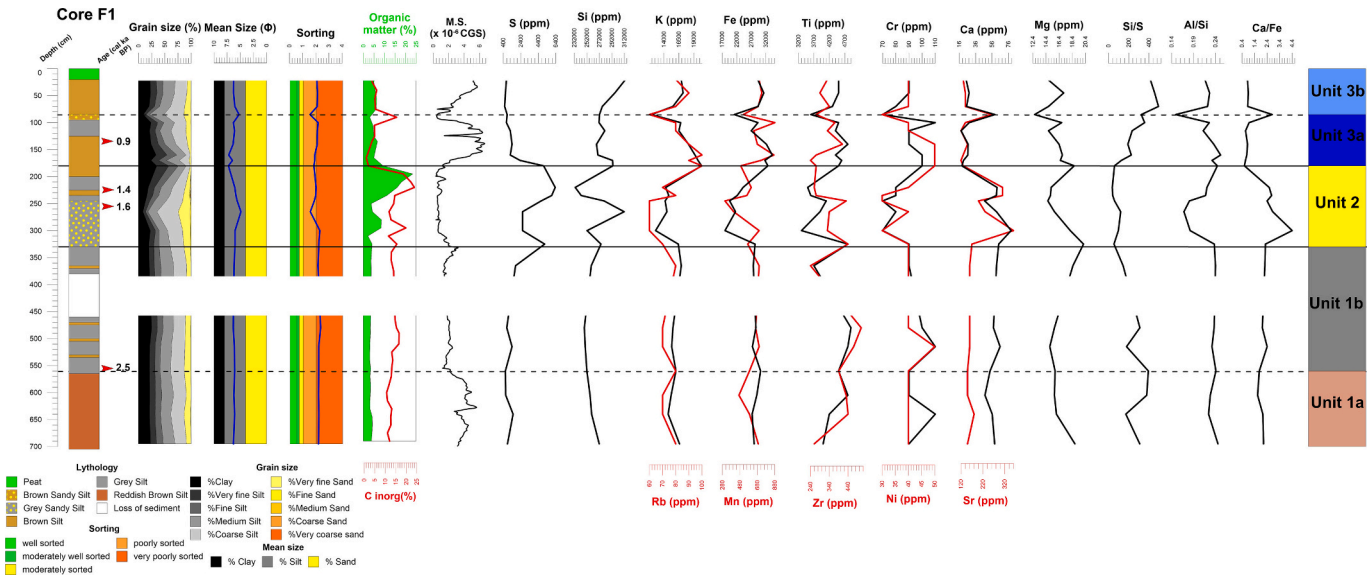

Fig. 2. Core F1 sediment properties, main geochemical elements content and corresponding lithological units. (M.S. stands for Magnetic Susceptibility).

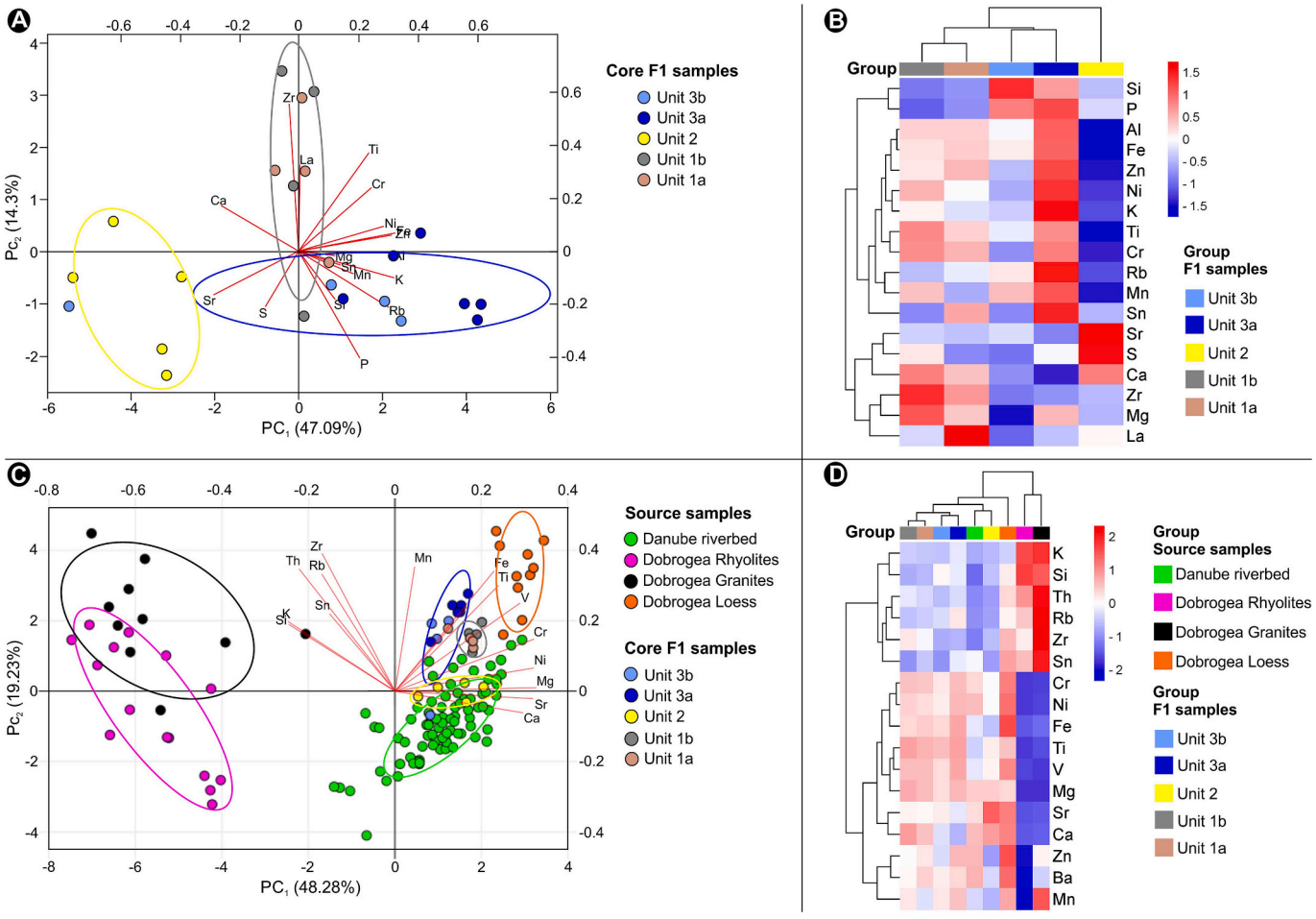

Fig. 3. (Left) PCA of main geochemical elements from core F1 (A), and from sediment sources plotted together with core F1 samples (C). The points represent the sediment samples with different colors belonging to different groups. Ellipses represent 68% confidence intervals of clusters core. Red lines represent the geochemical elements variables. (Right) Cluster heatmaps of main geochemical elements from F1 core (B) and from sediment sources plotted together with core F1 samples (D). The color coding indicates the high contents (red) versus the low contents (blue) in the sample hierarchy. Sediment sources sample values are from Scrieciu et al., 2023b (Danube riverbed), Seghedi et al., 1992 (Dobrogea Rhyolites), Întorsureanu et al., 1989 (Dobrogea Granites), Tugulan et al., 2016 (Dobrogea Loess). (For interpretation of the references to color in this figure legend, the reader is referred to the web version of this article.)

4.2. Sediment sources

Given its position near the Slava and Hamangia catchments, core F1 received material not only from the Danube but also from loess, granitic, and rhyolitic sources in central and northern Dobrogea. To assess the relative contributions of these sources through time, we first examined the internal geochemical variability of core F1 using principal component analysis (PCA) and then compared it with reference samples representing the main regional sediment sources.

A PCA performed on the core F1 geochemical data set yielded three distinct sample clusters, with the first two principal components (PC) explaining 61% of the total variance (Fig. 3A). These clusters correspond closely to the lithological units. Unit 1 samples plot mainly along PC2 (14% of the variance), reflecting elevated Zr and Mg contents, with additional contributions from Ti, Cr, and Ca (Fig. 3A, B). Units 2 and 3 cluster primarily along PC1 (49% of the variance), both showing negative scores on PC2. Unit 2 is characterized by high Sr and S, and secondarily Ca, whereas Unit 3 groups according to increased Si, P, Rb, K, and Mn, with subordinate contributions from Ni, Fe, Zn, and Al. To further constrain sediment provenance, the core F1 geochemical dataset was analyzed together with reference samples from the principal sediment sources in the region (Table 1). The first PCA axis provides a clear discrimination between the core F1, loess, and Danube riverbed samples and, on the opposite side, the granite and rhyolite samples from Dobrogea (Fig. 3C). The granite and rhyolite samples are rich in alkaline metals such as K and Rb, and in some transition metals such as Zr and Mn, and low in Sr, Ca, Ti, Mg, Fe, Cr, and Ni (Table 1). In contrast, Danube samples are rich in alkaline-earth metal such as Sr and Ca, and in transition metals as Mg, Ni, Cr, Zn, but low in granite and rhyolite specific elements. The loess samples are notably enriched in transition metals such as Fe, Ti, and V, while also containing elevated concentrations of elements commonly found in Danube riverbed sediments, including Sr, Ca, Zn, Cr, and Ni. In contrast, elements typically associated with the granitic and rhyolitic sources like K and Rb are present in small amounts.

On the factorial plane, the core F1 samples cluster close to the Danube riverbed and loess samples (Fig. 3C). However, each unit displays different compositions evidencing the contribution of multiple sources (Fig. 3D). Unit 1 exhibits a mixed Danube and Dobrogea geochemical signature. The lower Subunit 1a is dominated by loess (indicated by Fe and Ti), which is consistent with the reddish-brown silt color originating from iron-oxide or ferromagnesian minerals of loess deposits drained by Slava and Hamangia rivers. The Danubian source becomes dominant in Subunit 1b, evidenced by increases in Ca, Mg, and Sr contents and the change in color to typical Danube borne grey silts. Cr and Ni are slightly increased as well, though their source is ambiguous as they are abundant in both Danube sediments (Catianis et al., 2020; Catianis et al., 2018; Culicov et al., 2022; Dinescu et al., 2004) and loess deposits (Tugulan et al., 2016). Lesser contributions from Dobrogea granites and rhyolites are also reflected in Subunit 1b by the presence of Zr, Mn, and Th.

Unit 2 is entirely Danubian in origin with its samples clustering within the Danube riverbed reference samples (Fig. 3C), and sharing the same geochemical composition enriched in Sr and Ca while being low in most other elements (Fig. 3D). The enhanced Sr, Ca, and S are further amplified by local bioproduction which generated large quantities of organic matter and carbonates (Fig. 2).

Unit 3 contains mostly Dobrogea-borne sediments. The samples show a close geochemical relationship to Unit 1, particularly through the enrichment in loess-derived elements (Fe, Ni, Cr), with concentrations even higher than in Unit 1. The enrichment is consistent with the highest magnetic susceptibility values recorded in the core (Fig. 2). A key distinction in Unit 3, however, is the greater contribution from granitic and rhyolitic sources indicated by elevated levels of Rb, K, and Si. This input originates from the Slava River eroding the alkaline granite massif of Secaru Hill, which supplies Fe and Mg (from amphiboles and pyroxenes) and K and Rb (from potassic feldspars). In sharp contrast, the Danubian influence in Unit 3 is minimal, as this unit displays the lowest concentrations of Danube-derived elements in the entire core (Fig. 3D).

4.3. Faunal record

The samples from core F1 were analyzed for both microfauna (ostracods and foraminifers) and macrofauna (bivalves and gastropods) (Plates 1 and 2). The ostracod assemblage comprises 25 species belonging to 18 genera that were separated in three ecological groups – freshwater, brackish and marine - typical for deltaic settings where mixing of river water and marine flows is a common feature (Fig. 4). The associations are strongly dominated by the euryhaline *Cyprideis torosa*. The dominance of one species is typical for brackish lagoon environments, such as the Razelm-Sinoe, and the key for paleoecological interpretations is to evaluate the occurrences of the secondary, less abundant taxa (Frenzel and Boomer, 2005). The foraminifera assemblage is largely monospecific, dominated by *Ammonia tepida*, with only occasional occurrences of *Ammonia beccarii* tests. Foraminifers are good indicators of brackish waters, commonly found in lagoonal environments with mixing of oligo and mesohaline waters (Hayward, 2014). Due to the low diversity and the absence of clear morphological observations such as abnormal growth (Barbieri and Vaiani, 2018; Debenay et al., 2001), the relative abundance of foraminifers will be used in this study as a secondary proxy to refine paleosalinities primarily constrained by the ostracod assemblages. Macrofauna inspection revealed a number of 3 bivalve and 5 gastropod species, which were divided in the same three groups – freshwater, brackish and marine. The zoning of ostracod assemblages fits well with the lithological units; therefore, the faunal characteristics of each unit and subunit are described individually bellow.

Unit 1a is characterized by very low ostracod and mollusks abundances, with most samples containing only 5–20 valves, and others being entirely barren. The assemblage includes weak occurrences of the euryhaline *Cyprideis torosa*, freshwater specimens *Candona neglecta*, *Pseudocandona* sp., *Ilyocypris bradyi*, *Limnocythere inopinata*, *Heterocypris* sp., and few *Ammonia* spp. specimens. Few gastropod shells of *Ecrobia* and *Planorbis* and Charophyceae algae were encountered at 640 cm.

The boundary at 555 cm (marking Unit 1b) indicates a major change in ostracod fauna, transitioning to a monospecific association with *Cyprideis torosa* occurring in constant and overwhelming abundances (> 90%). Freshwater ostracods persist but are limited, featuring species such as *Candona neglecta* and *Pseudocandona compressa*. Foraminifers become more consistently present than in the previous unit, though still in very low numbers (< 10 valves). Macrofaunal analysis revealed frequent freshwater gastropods (*Ecrobia* sp. and *Planorbis* sp.), alongside occasional halotolerant *Dreissena* sp.

The beginning of Unit 2 marks a significant change: foraminifers become constant and abundant, mainly represented by *Ammonia* species (Fig. 4). Although *Cyprideis torosa* remains the dominant species, freshwater ostracod group increases in diversity (11 species, up from 8) and abundance toward the top, including notable occurrences of *Candona neglecta*, *Pseudocandona* sp., *Heterocypris* sp., *Pseudocandona albicans* and *Ilyocypris bradyi* (Plate 1). In the upper part few brackish species such as *Heterocythereis amnicola* and *Amnicythere pediformis* occur with very low abundances (< 10 valves). At the top, three mesohaline species are encountered: *Amnicythere multipunctata, Xestoleberis aurantia*, and *Cytherois cepa*. Macrofauna, predominantly freshwater taxa, includes bivalves like *Dreissena polymorpha* and gastropods like *Ecrobia* sp., *Theodoxus danubialis*, *Planorbarius corneus*. However, brackish bivalves (*Abra segmentum*, and *Cerastoderma* sp.) and the gastropod *Parthenina terebellum* dominate the assemblages at 245–270 and 195–200 cm intervals (Fig. 4, Plate 2).

The onset of Unit 3 marks another significant change in ostracod associations. The euryhaline *Cyprideis torosa* is still dominant, but the

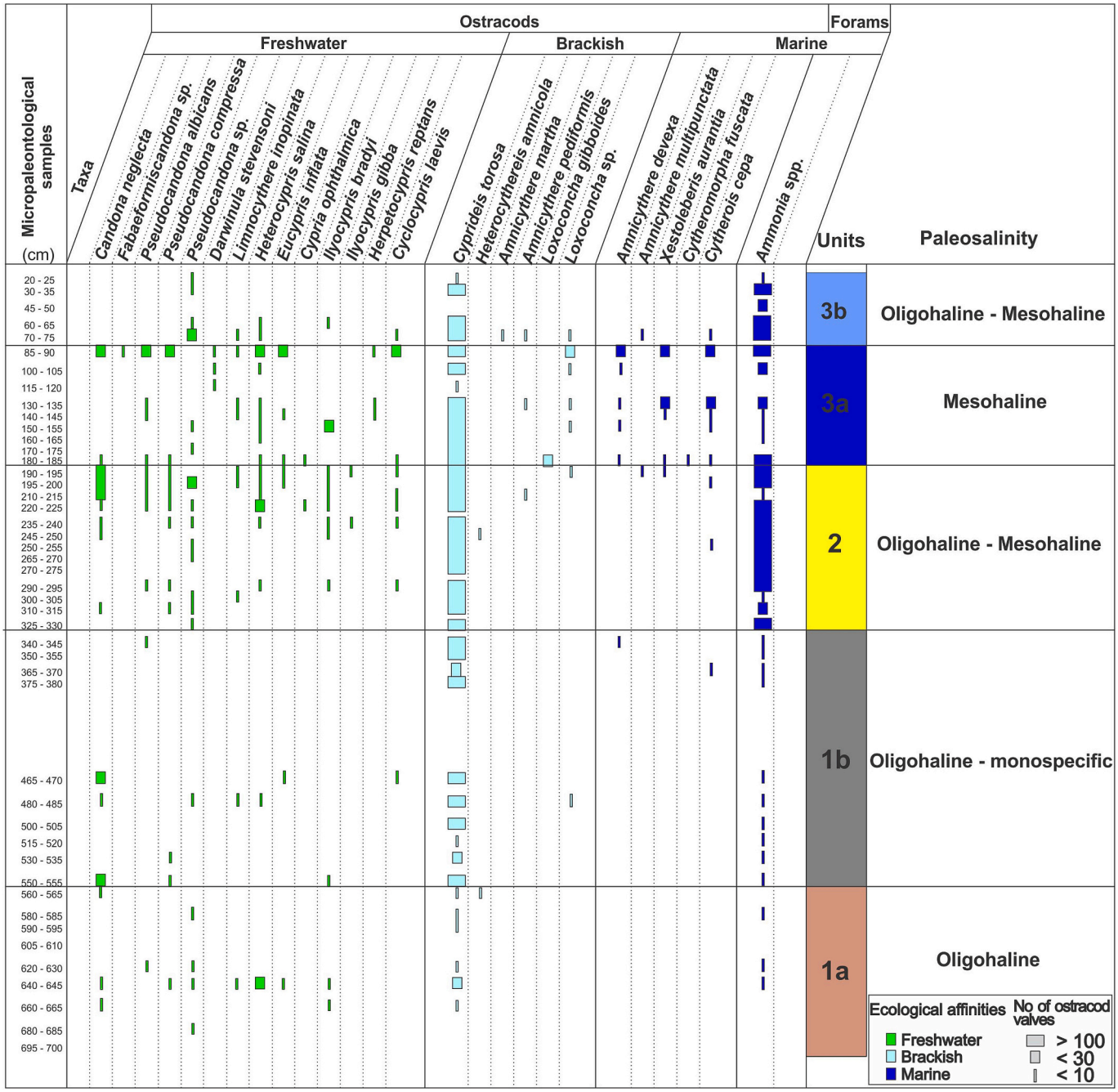

Fig. 4. Microfauna species and associations of core F1.

freshwater group is largely replaced by a diverse and abundant brackish – marine group. This includes mesohaline species such as *Amnicythere devexa*, *Cytherois cepa*, *Cytheromorpha fuscata* and lagoonal species such as *Xestoleberis* sp., *Loxoconcha gibboides* and *Amnicythere pediformis*. Foraminifers from the Ammonia genre remain but less abundant. The freshwater group decreases in diversity (8 species) and abundance with new entries such as *Darwinula stevensoni* and *Herpetocypris reptans*. The Candonidae group associated with stagnant waters in Unit 2, is almost entirely absent while species indicative of more lotic water bodies such as *Darwinula stevensoni* are noticeably present. Macrofauna, found only in the lower part, includes a mixture of well-preserved brackish (*Abra segmentum* and *Cerastoderma* sp., *Ecrobia* sp.) and freshwater taxa, (*Theodoxus danubialis* and *Planorbarius corneus*) (Plate 2).

The uppermost part of the core, Unit 3b records faunal decline. The assemblage still dominated by *Cyprideis torosa* gradually loses diversity and abundance toward the top where the last 25 cm are entirely void of fauna (Fig. 4). The remaining low – abundance fauna includes weak occurrences of freshwater taxa (*Pseudocandona* sp., *Heterocypris* sp.) and brackish species (*Amnicythere martha)*, with few isolated mesohaline taxa persisting (Fig. 4, Plate 1). Foraminifers like *Ammonia* sp. are present, butin low abundances. Macrofauna consists only of *Ecrobia* shells at 45 and 70 cm.

4.4. Chronology

The chronological framework of core F1 is based on four radiocarbon calibrated ages (Table 2). The base of the core and Unit 1a could not be dated due to the absence of suitable material. Although the available dates are stratigraphically coherent, the small number of samples limits the temporal resolution of the age–depth model.

To refine the age estimates at the boundaries between units, we modeled ages at the exact depths marking these transitions. The coring – related sediment loss between 380 and 460 cm introduces uncertainty in the age–depth model and in the precise timing of the depositional phases. However, outside the coring gap, the lithological characteristics indicate continuous sedimentation with consistent grain size and geochemical contents both immediately above and below the gap, and no observable hiatuses or erosional surfaces anywhere else in the core. Consequently, we assumed approximately continuous sedimentation and applied a simple linear interpolation. This approach provides modeled ages of 1787–2006 cal. yr BP at 325 cm (Unit 1b/Unit 2 boundary), 1140–1380 cal. yr BP at 187.5 cm (Unit2/Unit3a boundary), and 556–748 cal. yr BP at 85 cm (Unit 3a/Unit3b boundary). These modeled values should be regarded as approximations given the chronological limitations noted above. The age of the uppermost Unit 3a/Unit 3b boundary, which is above the youngest measured radiocarbon date, was derived through a limited extrapolation of the age–depth model to better constrain the timing of the uppermost stratigraphic boundary. The sediment surface was considered to represent present-day conditions (2021 CE, corresponding to the year of core retrieval).

5. Discussion

5.1. Mid to Late Holocene sediment fluxes in the RSLS

To analyze sediment fluxes in the lagoon system, we combined data from our core F1 (Acic Suat) with previously published cores: O2 (Bony et al., 2015), EN3 (Preoteasa et al., 2019), and C3, C6, C7, C10, C11, C13 (van de Velde et al., 2019) (Fig. 1). Sedimentation rates were calculated for each stratigraphic unit using both calibrated and modeled ages, and compared with previously published aggradation rates (Fig. 5). Our analysis focuses on sedimentation from ~6 ka BP onward, coinciding with the formation of the Razelm-Sinoe Lagoon system.

Between 6 and 2.6 ka BP sedimentation fluxes are documented by cores O2 (Orgame) and EN3 (Enisala) (Fig. 5). EN3 displays a low and continuous aggradation rate of 0.3 mm/year, lasting until 1.1 ka BP. In contrast, O2 records significant variability with an initial rate of 5.11 mm/year between 5.8 and 5.4 ka BP. This high rate reflects the first arrival of Danube sediments in the paleo-embayment, via the main Sfântu Gheorghe distributary. During 6–5.5 ka BP, this branch carried the entire sediment load of the Danube creating its first open sea lobe, bypassing the Dunavăț Promontory (Vespremeanu-Stroe et al., 2017). As the lobe spread radially, the main flow shifted predominantly eastward and only partially southward into the paleo-embayment. This change resulted in a significant threefold decrease in sedimentation rate – down to 1.88 mm/year – which persisted until around 4 ka BP.

Following a ~ 1000-year sedimentation hiatus at Orgame, deposition resumed around 3 ka BP with rates of 2.35–2.4 mm/year, continuing until 2.3 ka BP (Bony et al., 2015). This timing aligns closely with the onset of Dunavăț branch progradation in the paleo-embayment and its gradual seaward expansion (Vespremeanu-Stroe et al., 2017). Remarkably, the highest sedimentation rate in the system during this period was recorded further west at Acic Suat, where accumulation reached 3.4 mm/year between 2.6 and 1.9 ka BP. The exceptional rate of sedimentation in this hydrologically secluded sector of the lagoon strongly supports the presence of the Dunavăț distributary nearby. A marginal location could only accumulate sediment so rapidly through a sustained and direct supply, likely delivered via branching or spreading channels of the Dunavăț system. This interpretation is further reinforced by the geochemical and PCA evidence, both indicating a strong Danubian imprint in Subunit 1b.

After 2 ka BP sediment fluxes at Acic Suat decreased by about twofold, with rates dropping to 1.8–2 mm/year. A further decline occurred after 0.6 ka BP, reaching a minimum of 1.3 mm/year. At Orgame, sedimentation also fell sharply after 2.3 ka BP, decreasing to 0.6–0.8 mm/year by 0.3 ka BP. A similar reduction in sediment flux after

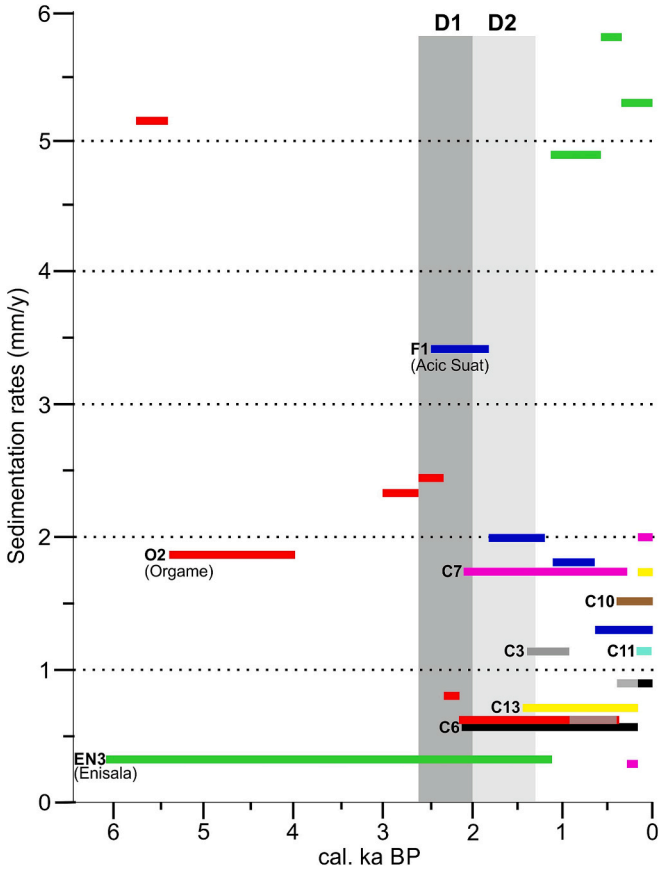

Fig. 5. Chronological representation of sedimentation rates across the RSLS. D1 and D2 represent the successive open sea lobes of Dunavăț branch. Cores from previous studies: EN3 (Preoteasa et al., 2019), O2 (Bony et al., 2015) and C3 – C13 (van de Velde et al., 2019).

2.3–1.9 ka BP is evident across most reviewed cores (Fig. 5). This system-wide decline corresponds to the formation of Dunavăț 2 (2–1.3 ka BP), which developed south of the earlier lobe following major Danube avulsions around 2 ka BP (Vespremeanu-Stroe et al., 2017). Dunavăț 2 lobe had a larger areal than Dunavăț 1, implying that more sediment was trapped and deposited within the lobe itself (Vespremeanu-Stroe et al., 2013). Consequently, less sediment reached the lagoon, particularly its marginal areas, leading to weaker sediment fluxes than during the older Dunavăț stage. Cores such as C6, C13, O2 (western bank) or C13 (Portita outlet) show similarly low rates of 0.6–0.8 mm/year while C7 (eastern bank) and F1 (Acic Suat) record higher rates of 1.7–2 mm/year but still within the overall declining trend. These higher values reflect proximity to additional sediment sources – secondary delta channels in the case of C7 and local bioproduction in the case of F1 – which partly compensated for the broader sediment depletion caused by the Dunavăț branch. As previously mentioned, the Enisala area remained largely isolated from significant sediment inputs with accumulation rates near 0.35 mm/year throughout most of the Mid to Late Holocene. Its position on the western edge of the lagoon, opposite the main southward sediment transport pathways of the Dunavăț branch, limited deposition. Powerful northern winds characteristic of the region likely further deflected sediments away from Enisala, further exacerbating its sediment-starved conditions.

Finally, during the last millennium, sedimentation rates increased across most cores. In the Enisala area, rates rose 10 to 15 above earlier values (Preoteasa et al., 2019reflecting a shift from silicilastic deposition to in situ biogenic production as Danubian sediment input declined and wetlands expanded along the RSLS margins.

5.2. Paleogeographic reconstruction of the western coast of Golovița Lake and its implications for the evolution of the Razelm-Sinoe lagoon system (RSLS)

The integrated multi-proxy data from core F1 allows for the reconstruction of five key paleoenvironmental phases spanning the Late Holocene evolution of the western RSLS.

5.2.1. Protected embayment with intense river input (unit 1a): pre 2.5 ka BP

The high concentrations of terrigenous elements (Ti, Fe, Cr, Zr,) and elevated magnetic susceptibility (MS), combined with low organic matter (OM) and sulfur (S), indicate sustained siliciclastic input into the paleoembayment. The geochemical signature is consistent with a Dobrogean source, reflected also in the reddish-brown sediments derived from the Slava and Hamangia rivers. The limited abundance and diversity of fauna, (ostracods and mollusks) further support a river-dominated, low-salinity setting (Figs. 4 and 6).

Although Subunit 1a is dated only at its upper boundary (2.6 ka BP), it most likely corresponds to the early expansion of the Dunavăț distributary into the RSLS. This aligns with the broader deltaic reorganization that followed the decline of the Sfântu Gheorghe 1 lobe and the subsequent avulsions redirecting flow toward the southern delta (Vespremeanu-Stroe et al., 2017). During this phase, the RSLS remained semi-enclosed but still connected to the Black Seain its southern sector between the Sfantu Gheorghe 1 lobe and the Zmeica barrier (Fig. 7A). The Zmeica Barrier, initiated around 5–4.5 ka BP (Giosan et al., 2006, Vespremeanu-Stroe et al., 2017 had already formed as a shallow, wave-built feature fed by downdrift transport from the Sfântu Gheorghe 1 lobe. By the time Unit 1a accumulated, it was sufficiently developed to limit marine inflows and contribute to the oligohaline conditions reflected by the microfaunal assemblage. These assemblages – dominated by *Cyprideis torosa*, Candonidae, and freshwater gastropods (Ecrobia, Planorbis) – indicate low salinity, while the sparse foraminiferal presence likely represents residual populations surviving from earlier mesohaline phases (Preoteasa et al., 2019).

Overall, the geochemical and faunal evidence shows that Unit 1a formed within an oligohaline, river–influenced embayment (Fig. 6). Inputs came primarily from nearby Dobrogean rivers reinforced by the freshwater influence of the advancing Dunavăț branch, while the Zmeica Barrier played a key role in restricting saline intrusions (Fig. 7A).

5.2.2. Oligohaline lagoon with narrow outlets (unit 1b): 2.5–1.9 ka BP

Unit 1b records a transition to typical grey Danube-borne silts, with Ca – Mg enrichment indicating intensified input from the Dunavăț distributary. Minor geochemical signals of Zr, Mn, and Th reflect secondary contributions from the Slava and Hamangia rivers. The faunal shift toward high proportions of *Cyprideis torosa* signals the establishment of an oligohaline lagoon receiving substantial freshwater input but with restricted marine exchange.

Chronologicaly, this phase corresponds to the progradation of the Dunavăț 1 lobe (2.6–2 ka BP), which closed the RSL around 2.6 ka BP and left only a narrow marine, most likely through a small outlet acoss the downdrift Lupilor barrier (Figs. 6 and 7B). This hydrological configuration – high freshwater input and limited salinity intrusion – is consistent with the proliferation of *Cyprideis torosa,* elevated proportions of oligohaline ostracods, and the occurrence of freshwater mollusks (*Dresissena* sp. and *Planorbis* sp.). The persistence of a small number of foraminifers reflects a residual, stressed population surviving in these increasingly oligohaline conditions. The high sedimentation rate at Acic Suat (3.4 mm/y) reinforces the proximity and influence of the Dunavăț distributary, implying sustained sediment supply through branching channels even in secluded sectors of the lagoon.

5.2.3. Oligo to mesohaline lagoon with constant marine inflows (unit 2): 1.9–1.2 ka BP

Unit 2 marks a shift from dominantly terrigenous to increasingly organic-rich, carbonate- sediments, reflected by declining Dobrogean geochemical signatures (Rb, K, Fe, Ti) and higher OM and Ca/Fe ratios (Figs. 3 and 6). At the same time, increases in Sr, and episodic rises in Ca and Mg, indicate continued but fluctuating Danubian input, likely linked to hydrological reorganization following the avulsion of the Dunavăț distributary around 2 ka BP.

Although the newly formed Dunavăț 2 lobe developed closer to the core site, sedimentation rates to ~2 mm/year (Fig. 5). This reduction likely reflects the rapid seaward progradation of the new lobe, which concentrated sediment at its marine front rather than within the lagoon. The fast buildup of Dunavăț 2 – documented by Saele and Chituc beach

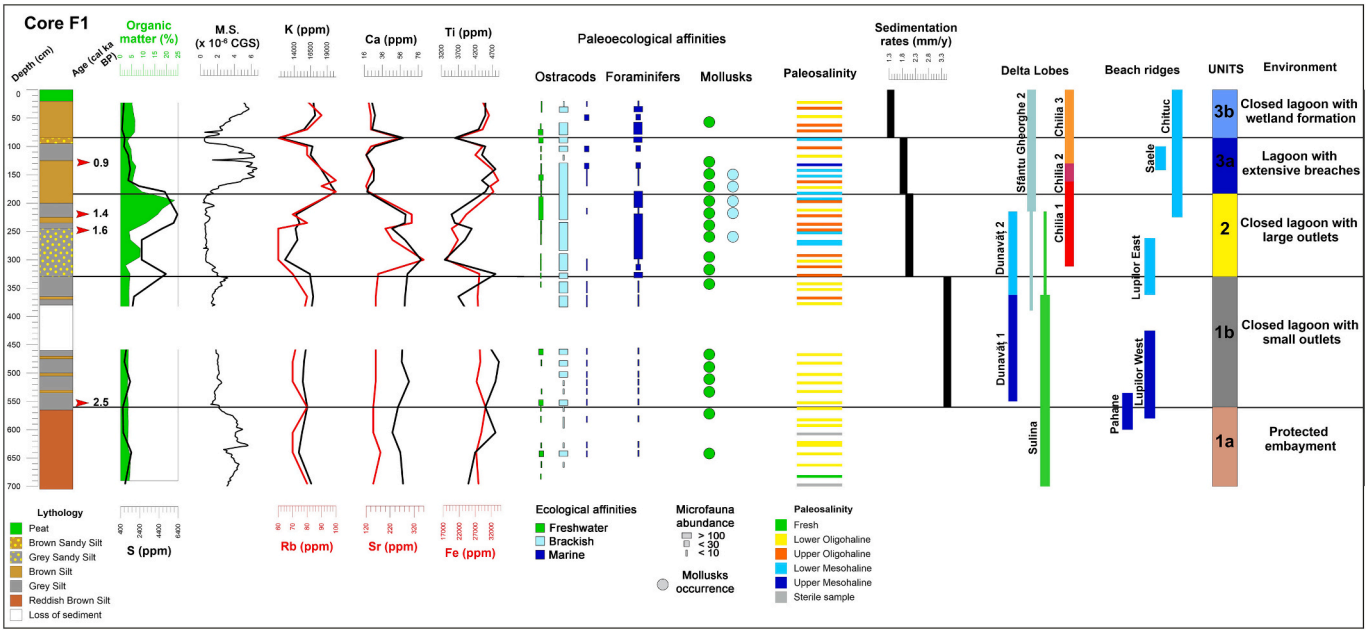

Fig. 6. Integrated multi-proxy analysis of core F1 and paleoenvironmental interpretation. Danube delta lobe chronology is from Vespremeanu-Stroe et al. (2017), and beach ridge chronology from Vespremeanu-Stroe et al. (2016).

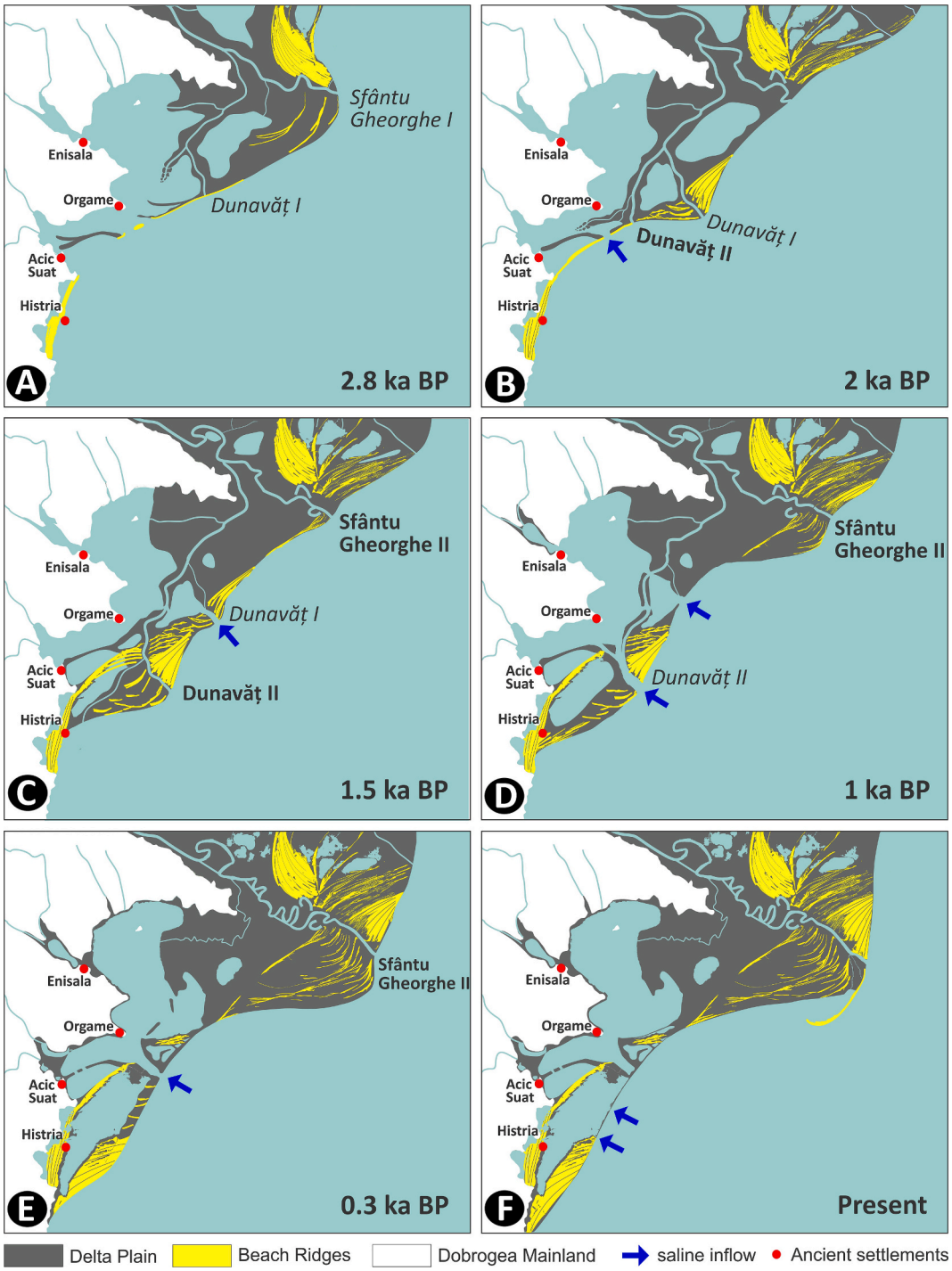

Fig. 7. Evolutionary stages of the Razelm-Sinoe lagoon system (modified after Vespremeanu-Stroe et al., 2017): (A) Closing of the initial paleoembayment and Dunavăț branch advancement into the RSLS (2.8 ka BP), (B) Dunavăț 1 lobe largest expansion (2 ka BP), (C) Dunavăț 2 lobe progradation and erosion of Dunavăț 1 lobe (1.5 ka BP), (D) Dunavăț 2 lobe erosion and complete degradation of Dunavăț 1 lobe (1 ka BP), (E) Dunavăț 2 lobe canibalization (0.3 ka BP), (F) present configuration. The names in bold font are of active lobes, while italic font is for inactive lobes.

ridges progradation rates of 10–14 m/year (Vespremeanu-Stroe et al., 2013) – also contributed to the progressive clogging of maritime access near the ancient city of Histria (Istros) and reduced lateral sediment delivery into the RSLS. By ~1.5 ka BP, a sharp rise in OM and S contents indicates a transition toward lower-energy, biogenic dominated accumulation as detrital flux diminished.

Microfaunal assemblages reinforce this environmental shift. Foraminifera become more abundant, brackish and marine ostracods appear for the first time, and freshwater species remain present but more diverse (Figs. 3, 6). Together with the continued dominance of *Cyprideis torosa*, these changes indicate an oligo- to mesohaline lagoon with regular but controlled marine inflows. Such conditions are consistent with a largely closed Razelm lagoon that maintained periodic saline exchange through large outlets, most probably through the regressive, partially eroded mouth of the earlier Dunavăț 1 lobe (Fig. 7C).

5.2.4. Mesohaline lagoon with large breaches (unit 3a): 1.2–0.6 ka BP

Geochemical analysis shows a renewed peak in terrigenous elements

and MS indicating intensified siliciclastic deposition. Elevated Rb and K values, together with a shift to brown colored sediment point to the reactivation of the Dobrogean sediment source (Fig. 3). Despite this, the sedimentation rate of ~1.8 mm/yr, reflect the broader decrease in Danubian input to the RSLS. Even so, the Acic Suat area maintained comparatively higher aggradation than many other sites due to continued supply from the local Dobrogean rivers (Fig. 5). The abandonment of the Dunavăț 2 lobe around 1.3 ka BP shifted the main Danube flow back toward the Sfântu Gheorghe arm (Vespremeanu-Stroe et al., 2013, 2017) significantly reducing sediment flux into the lagoon. These dynamic geomorphological changes impacted as well the paleoecological conditions in the area which in turn affected the ostracod assemblages. *Cyprideis torosa* remains dominant but secondary taxa shift significantly: freshwater species decline while brackish and marine taxa become increasingly common (Figs. 3, 6). The appearance of marine and coastal species such as *Cytheromorpha fuscata* and *Amnicythere multipunctata* together with marine opportunists such as *Abra segmentum* and *Cerastoderma glaucum*, suggests constant saline inflows likely facilitated by large breaches formed through the erosion of former Dunavăț 1 and 2 river mouths. The disappearance of the Candonidae group and the arrival of *Darwinula stevensoni* further suggest enhanced water circulation driven by wave activity inside the lagoon. As Dunavăț 2 was abandoned, sediment flux was redirected to the developing Sfântu Gheorghe 2 lobe, leaving the southern RSLS coast sediment-starved and increasingly vulnerable to intense erosion and breach initiation (Fig. 7D).

5.2.5. Closed oligo – Mesohaline lagoon with marginal wetland formation (unit 3b): 0.6 ka BP – Present

The uppermost unit begins with a decline in terrigenous element content and MS values, which then gradually increase toward the top (Figs. 2, 6). Several peaks in Rb and Mn, along with brown-colored sediments, indicate input from Dobrogea rivers over a weak Danube influence, consistent with the unit's lowest sedimentation rate of 1.3 mm/year (Fig. 5). Microfaunal assemblages show progressive freshening: an initial mix of freshwater, brackish, and marine species is followed by the abrupt disappearance of freshwater specimens and a subsequent decline in their abundance and diversity upward. *Cyprideis torosa* and foraminifers also decrease, while macrofauna remains scarce, limited to few *Ecrobia* sp. occurrences (Figs. 3, 6). Throughout the unit, fragmented mollusk shells and plant remains (seeds, roots, reed scraps and small wood fragments) are present, and the uppermost 20 cm consist of peat devoid of fauna. These characteristics signal gradual silting of the embayment, and a shift from aquatic to marginal marsh deposition.

In a geomorphological context, these transformations took place in the aftermath of Dunavăț 2 lobe erosion, when NE-directed longshore transport reshaped the southern deltaic coast as it adjusted toward a new coastal equilibrium (Fig. 7E). This gradually led to the present-day coastal configuration, with the amalgamated ridges of Saele-Chituc in the far south, resulted from the cannibalization of Dunavăț 2 lobe, a narrow barrier in the median part, and the remnants of the Pahane-Ranec ridges. This reworking progressively clogged of former large breaches, leaving only a few isolated narrow openings.

5.3. Reconstruction of extreme storms periods in the RSLS during the last 1500 years

Previous studies indicate that mesohaline conditions developed in the RSLS around the same time as the deposition of Unit 4 in core F1. The presence of high-salinity waters at several, distant sites along the western bank – yet occurring simultaneously between 1.5 and 0.6 ka BP within an otherwise closed lagoonal, implies a sustained connection to the Black Sea. Such a connection likely enabled consistent and substantial marine inflows to penetrate deep into the lagoon, most plausibly through large breaches. Given the geomorphological configuration of the RSLS during this period, such breaches could have been produced and maintained only by extreme storm events or prolonged periods of high storminess.

Modern storms in the NW Black Sea can generate offshore waves up to 7 m and are capable of breaching barriers and reshaping the coastline (Zăinescu et al., 2017, 2019). Assuming similar storm intensities in the past – particularly along the sediment-starved coast that developed after the cessation of Dunavăț 2 progradation around 1.3 ka BP – barrier failures would have been highly probable. Such openings would have allowed pulses of saline water to penetrate deep into the lagoon. Additionally, the configuration of the coastline prior to the full extension of the Sfântu Gheorghe 2 lobe exposed the barrier more directly to dominant NE–SW storm winds, further increasing the likelihood of repeated barrier breaches and significant saline intrusions.

By correlating the ages of mesohaline faunal assemblages in our core with those from previously published records, we attempted to constrain the timing of these possible intense storm periods that affected the southern Danube Delta coast over the past 1500 years. Using a correlation framework that required at least three cores – with a minimum of two showing no less than lower mesohaline conditions, and a third at least upper oligohaline conditions –we identified four high salinity intervals (HS): 1.53–1.45, 1.32–1.2, 0.95–0.89, and 0.67–0.63 ka BP – which we attribute to episodes of enhanced storm activity (Fig. 8). The first high salinity interval (HS1–1.53–1.45 ka BP) is concurrent with the maximum extension of Dunavăț 2 lobe and the erosion of Dunavăț 1, likely channeling saline inflows through the breached river mouth and impacting lagoon ecology (Fig. 7). Cores F1 (Acic Suat), C11 (Golovița) and O2 (Orgame) show mesohaline faunal changes with species such as *Amnicythere pedifomis* in F1 and various *Amnicythere* and *Loxoconcha* species in O2. The second high salinity interval (HS2–1.32–1.2 ka BP) is synchronous with the cessation of Dunavăț 2 lobe progradation, making the RSLS a mesohaline lagoon as seen in core F1 coastal and marine ostracods. This period, also observed at Orgame, includes storm evidence, such as *Buccinum undatum* shells (Bony et al., 2015), correlating with mesohaline conditions at Acic Suat. Between 1.3 and 1.2 ka BP, high salinity ostracod specimens (*C. fuscata*, *A. multipunctata, Loxoconcha eliptica)* and brackish species (*Cyprideis torosa*, *Amnicythere quinquetuberculata*, *Loxoconcha gibboides*) were found both in Acic Suat and Orgame cores (Fig. 8). The third high salinity interval (HS3: 0.95–0.89 ka BP) shows the highest estimated salinity with abundant marine specimens in all three, including *Xestoleberis aurantia* and *Cytherois cepa* in Acic Suat and *Cytheromorpha fuscata* and *Amnicythere histriana* in Enisala core. Brackish species such as *C. torosa* and *A. pediformis* appear in both, while certain species like *Loxoconcha. gibboides* and *Amnicythere. cymbula* were identified only in Enisala. Marine bivalves such as *Abra segmentum* and *Cerastoderma glaucum* are widespread, with others like *Mytilus galloprovincialis* and *Mytilaster minimus* recorded in specific cores. The most recent high salinity interval (HS4: 0.67–0.63 ka BP) features dominant euryhaline ostracods (*Cyprideis torosa* in Acic Suat and *T. amnicola* in Enisala) and significant marine species at Acic Suat, while Enisala mostly shows brackish taxa.

In the absence of local paleostorm records, we compared our results with several high-resolution archives that reconstruct past storm activity using different proxies: the Bagnas Lagoon record from the western Mediterranean, based on strontium concentrations in sediments (Degeai et al., 2015); the multi-proxy core from Pierre-Blanche Lagoon, which integrates grain size, geochemistry, clay mineralogy and faunal analyses (Sabatier et al., 2012); high-energy estuarine and coastal sedimentary records from the northwestern Europe (Sorrel et al., 2012); and a North Atlantic Oscillation (NAO) index reconstructed for the past millennium, from 48 annually resolved proxy datasets distributed across the Atlantic basin (Ortega et al., 2015).

The high-salinity intervals identified in the RSLS record – interpreted as phases of intensified storm activity (HS1, HS2, and HS4) – correspond closely to storm phases SP6, SP5, and SP3 in the Bagnas sequence (Fig. 8). The storm period reconstructed at 1950–1400 cal. yr BP in the

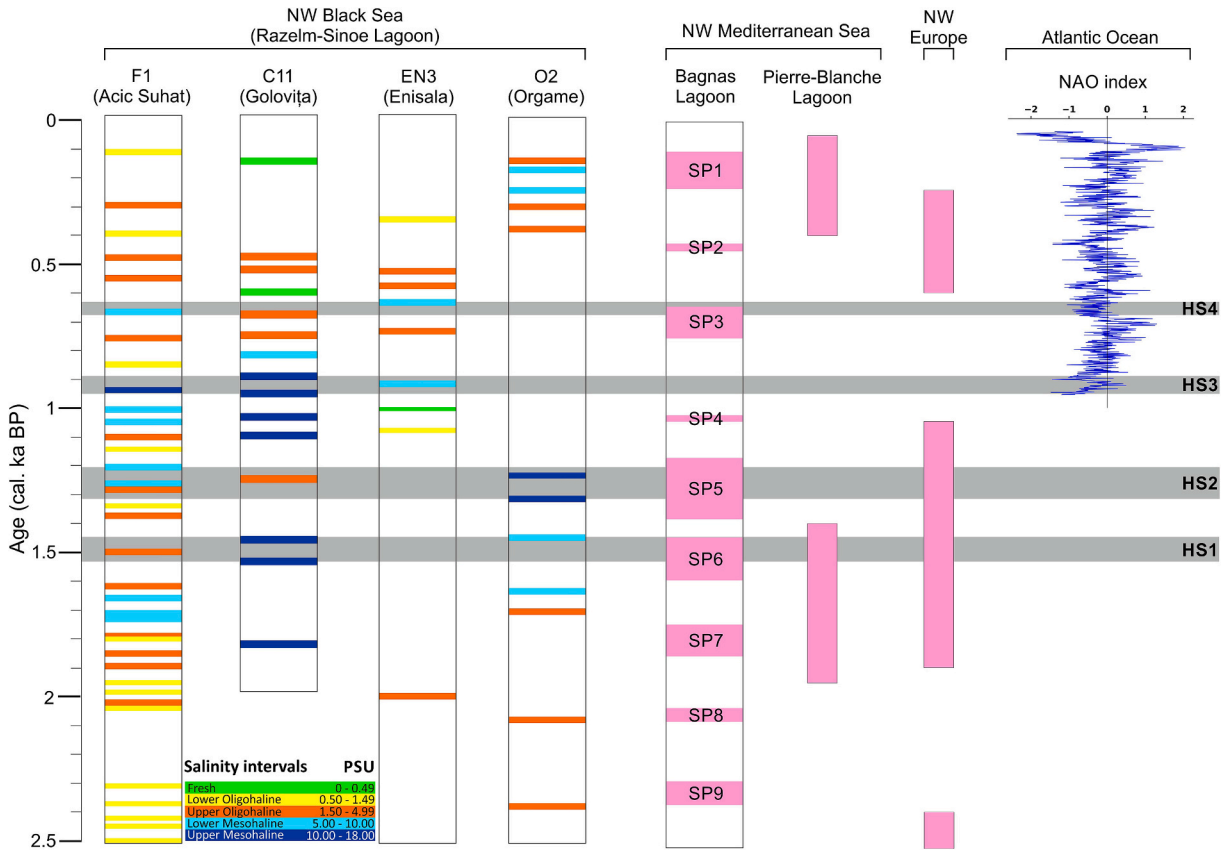

Fig. 8. Temporal correlations of mesohaline faunal associations in the Razelm-Sinoe Lagoon System (RSLS) and comparison with paleoclimatic proxies. RSLS cores include EN3 (Preoteasa et al., 2019), O2 (Bony et al., 2015), and C11 (van de Velde et al., 2019). Paleoclimatic records comprise: reconstructed storm periods (SP) from the Bagnas Lagoon (Degeai et al., 2015), periods of high storm activity from the Pierre-Blanche Lagoon (Sabatier et al., 2012), Holocene storm periods from northwestern Europe (Sorrel et al., 2012), and a NAO index derived from 48 annually resolved proxy datasets distributed across the Atlantic basin (Ortega et al., 2015). Grey horizontal bars indicate the reconstructed high-salinity intervals (HS) within the RSLS, while pink vertical bars represent the reconstructed storm periods in the proxy records. The salinity intervals of the cores samples within the RSLS are from van de Velde et al., 2019. (For interpretation of the references to color in this figure legend, the reader is referred to the web version of this article.)

Pierre-Blanche Lagoon correlates primarily with HS1, whereas the northwestern Europe second earliest storm record aligns not only with HS1 but also with HS2. These correspondences suggest a notable coherence between storm activity in Western Europe and the Northwestern Black Sea. Comparisons with the NAO reconstruction indicate that HS3 and HS4 coincide with negative NAO phases, consistent with previous studies linking enhanced modern storminess along the Danube delta coast to negative or near-zero NAO values (Vespremeanu-Stroe et al., 2007; Vespremeanu-Stroe and Tătui, 2011). However, recent research emphasizes that additional climate modes, including the East Atlantic (EA) and East Atlantic–Western Russia (EAWR) patterns, also influence recent storminess in the northwestern Black Sea (Zăinescu et al., 2017). This complicates direct comparisons with Mediterranean records, where similarly to the Black Sea, multi-centennial storm variability cannot be attributed to NAO dynamics alone (Degeai et al., 2015), indicating that different atmospheric mechanisms operate in each region.

We note that the storm reconstructions proposed here are indirect, relying on salinity shifts and mesohaline faunal changes rather than on discrete sedimentological storm layers (e.g., coarse event beds or sand laminae). This likely reflects the depositional setting of the investigated cores. Core F1 is located in a sheltered and isolated sector of the RSLS, approximately 20 km from the nearest present-day marine outlet. Throughout much of its evolution, it was situated at a considerable distance from active marine outlets and direct marine influence, likely even farther than at present due to change in the configuration of the coastal system. Under these low-energy conditions, sediment grain-size and sorting remain relatively uniform, while sedimentary signatures of storm events are largely absent. A similar situation applies to the other cores included in the correlation framework, which are also situated along the mainland margin of the lagoon, far from the coastal barrier where storm-induced overwash and coarse-grained deposits would be expected to accumulate. Consequently, storm activity is recorded primarily through hydrological and ecological responses of the lagoon system rather than through the preservation of distinct event layers. This limits the ability to distinguish individual events from longer periods of enhanced storminess. Future high-resolution cores targeting stratigraphic evidence of overwash or storm-deposited layers are needed to validate and refine these intervals and to more precisely link them to specific modes of atmospheric circulation. Furthermore, cross-site comparisons with regional archives strengthen the interpretation of RSLS environmental phases. However, differences in chronological frameworks, sampling resolutions, and analytical approaches across studies introduce uncertainty and may limit exact temporal alignment between the salinity corelations, therefore they should be regarded as broadly contemporaneous rather than strictly synchronous.

5.4. Human-landscape interactions in the southern Danube delta during the Late Holocene

The findings from the Acic-Suat site highlight an environmental trajectory closely aligned with that of Orgame, shaped by their shared location within the Razelm-Sinoe lagoon system and their exposure to similar environmental forces. Both settlements were influenced by the

progradation of the Dunavăț branch, which gradually decoupled them from direct access to the open sea. However, this geomorphological evolution did not isolate them entirely. Instead, navigation and regional trade were sustained via the Dunavăț 1 and 2 branches, preserving maritime connectivity deep into the first millennium CE. This reinforces the view that lagoonal buffering, combined with access to evolving fluvial networks, contributed to the longevity and adaptability of these coastal settlements.

This regional context is further clarified by comparing the environmental histories of the major Greek colonies of Orgame and Histria (Istros). Both were founded in the mid-7th century BCE, yet their long-term development diverged significantly due to differences in coastal positioning and sedimentary regimes (Bony et al., 2015; Vespremeanu-Stroe et al., 2013). Orgame was located behind the Zmeica barrier, in a naturally protected lagoon that provided a stable harbor environment. From its foundation until the beginning of the Hellenistic period (6th to 4th century BCE), maritime access was maintained through a wide natural outlet between the southern tip of the Sfântu Gheorghe I lobe and the Zmeica barrier. As the Dunavăț lobe began to prograde during the Hellenistic period, the outlet remained active, although its configuration evolved becoming narrower due to the downdrift development of the Lupilor barrier further enclosing the lagoon in the south. In the Roman period (1st to 7th century CE), after the abandonment of the Dunavăț 1 lobe and the progradation of Dunavăț 2, the harbor retained its functionality – either through continued use of outlets via breaches in the older lobe or through the active Dunavăț 2 distributary. By contrast, Histria was established on a low-lying coastal barrier exposed to more dynamic sedimentation. The subsequent formation of the Chituc barrier following the erosion of Dunavăț 2 lobe progressively infilled its harbor, which by Late Antiquity was left far inland by the fast-prograding coast and lost its maritime utility. This ultimately contributed to the decline and abandonment of the city (Vespremeanu-Stroe et al., 2013).

These environmental contrasts shaped the social and economic paths of the two settlements. Histria flourished early due to its direct access to the Black Sea and developed urban structure, whereas Orgame remained more modest but resilient, thanks to its more stable lagoonal setting. The parallel trajectory of Acic-Suat, as revealed in this study, emphasizes the importance of lagoonal environments in supporting long-term habitation, navigation, and adaptation in the face of changing deltaic dynamics. While these reconstructions highlight meaningful correspondences between environmental phases and settlement histories, the links remain interpretative. The correlations rely primarily on spatial proximity and broad chronological overlap rather than on direct archaeological – sedimentary associations. Establishing a definitive causal relationship between lagoonal evolution and settlement dynamics will require integrated geoarchaeological excavation and stratigraphic work at the sites themselves.

Together, these cases demonstrate how natural processes and environmental thresholds played a central role in structuring the historical geography of Greek colonial landscapes in the western Black Sea.

6. Conclusions

The study at Acic-Suat provides new insights into the Late Holocene evolution of the Razelm-Sinoe Lagoon System (RSLS), highlighting the influence of the southernmost Danube distributary, the Dunavăț branch. Sedimentological and paleoecological evidence reveals dynamic interactions between fluvial input, local biogenic accumulation, and lagoonal processes, with sedimentation rates declining after lobe switching and final abandonment (~2–1.3 ka BP). Five main phases of lagoonal evolution over the last ~3000 years are identified, ranging from a fluvially influenced embayment to a closed oligo- to mesohaline lagoon. Correlated mesohaline faunal assemblages across multiple cores reveal four storm-driven breaching intervals (~1.4–1.5, 1.2–1.3, 0.9–1.0, and 0.6–0.7 ka BP), emphasizing the lagoon's sensitivity to extreme events. Although sites like Acic-Suat may not individually yield major historical revelations, their geoarchaeological potential lies in refining broader regional narratives. Situated between the prominent Greek colonies of Istros and Orgame, Acic Suat contributes to our understanding of how smaller settlements responded to fluctuating hydrological conditions, shifting coastlines, and variable resource availability. Framed through a multi-proxy, geoarchaeological approach, such sites help reconstruct the nuanced interactions between human communities and their changing landscapes during the Late Holocene.

Beyond the local context, the findings have wider implications for coastal and deltaic research. The study enhances understanding of distributary – controlled sedimentation, lagoon closure and reopening cycles, and storm-induced coastal reconfiguration – processes that are central to the geomorphological evolution of many Black Sea, Mediterranean, and global delta-bounded lagoons. The reconstructed paleostorm chronology also provides a valuable benchmark for assessing the long-term recurrence, magnitude, and ecological impacts of extreme coastal events. Furthermore, the use of ostracod assemblages to identify storm-driven mesohaline incursions illustrates their potential as proxies for high-energy coastal events, contributing to the development of paleostorm reconstructions research.

At the same time, several limitations must be acknowledged. The interpretations rely on a single core with a limited number of radiocarbon ages. These constraints underscore the need for multi-core transects, denser chronologies, and expanded multiproxy datasets to refine spatial patterns of lagoonal change and to strengthen regional correlations. Future work integrating sedimentology, paleoecology, geochemistry, and high-resolution chronological modelling will be essential for advancing RSLS reconstructions.

Finally, this study demonstrates the methodological value of combining detailed sedimentary facies analysis with faunal, geochemical, and geoarchaeological data. This cross-disciplinary framework, applied here for the first time at Acic-Suat, provides a robust template for future investigations seeking to unravel the complex interactions among fluvial dynamics, coastal processes, and human activity in the RSLS and comparable delta- influenced lagoon systems.

CRediT authorship contribution statement

Sabin Rotaru: Conceptualization, Formal analysis, Writing – original draft, Writing – review & editing, Visualization. **Radu George Dimitriu:** Formal analysis. **Dan Vasiliu:** Formal analysis. **Bogdan Barbu:** Formal analysis. **Bogdan Ispas:** Formal analysis. **Andrei Briceag:** Writing – review & editing, Visualization, Formal analysis.

Funding sources

This research was funded by the Project PNRR C9 - I8 “Multiproxy reconstruction of Eurasian Megalakes, connectivity and isolation patterns during Neogene-Quaternary times”, code 97/15.11.2022, Contract No. 760115/23.05.2023.

Declaration of competing interest

The authors declare that they have no known competing financial interests or personal relationships that could have appeared to influence the work reported in this paper.

Acknowledgements

We are grateful to Dr. Antoneta Seghedi (GeoEcoMar) for fruitful discussions regarding the geology and tectonics of Dobrogea region. We thank our colleagues Ion Stanescu and Dr. Irina Stanciu for valuable fieldwork assistance. We are grateful to the two anonymous reviewers, who made very useful comments and suggestions, greatly improving the clarity and coherence of the manuscript.

References

Antipa, G., 1914. Câteva probleme Ştiinţifice şi economice privitoare la Delta Dunării. An. Acad. Rom. Mem. Sect. St. 2 (36), 61–135.

Baralis, A., Lungu, V., Dupont, P., Bastide, M., Bony, G., Caraire, G., Comfort, A., Delfieu, R., Guy, M., Jubeau, T., David, K., 2017. L'établissement d'Acic-Suat (commune de Baia, département de Tulcea). Méthodologie d'une enquête pluridisciplinaire. Pontica L, 455–488.

Barbieri, G., Vaiani, S.C., 2018. Benthic foraminifera or Ostracoda? Comparing the accuracy of palaeoenvironmental indicators from a Pleistocene lagoon of the Romagna coastal plain (Italy). J. Micropalaeontol. 37 (1), 203–230.

Bivolaru, A., Bottez, V., Asăndulesei, A., Vladu, A., Sava, T., Giaime, M., Morhange, C., 2021. Istros, Black Sea Coast, Romania A Geoarchaeological Perspective on the Location of the Harbour (S). In: Under the Mediterranean I: Studies in Maritime Archaeology.

Blott, S.J., Pye, K., 2001. GRADISTAT: a grain size distribution and statistics package for the analysis of unconsolidated sediments. Earth Surf. Process. Landf. 26 (11), 1237–1248.

Bony, G., Morhange, C., Marriner, N., Baralis, A., Kaniewski, D., Rossignol, I., Lungu, V., 2015. History and influence of the Danube delta lobes on the evolution of the ancient harbour of Orgame (Dobrogea, Romania). J. Archaeol. Sci. 61, 186–203.

Briceag, A., Ion, G., 2014. Holocene ostracod and foraminiferal assemblages of the Romanian Black Sea shelf. Quat. Int. 345, 119–129.

Briceag, A., Yanchilina, A., Ryan, W.B., Stoica, M., Melinte-Dobrinescu, M.C., 2019. Late Pleistocene to Holocene paleoenvironmental changes in the NW Black Sea. J. Quat. Sci. 34 (2), 87–100.

Bronk Ramsey, C., 2001. Development of the Radiocarbon Calibration Program. Radiocarbon 43, 355–363 (Proceedings of 17th International 14C Conference).

Caraion, F.E., 1967. Familia Cytheridae (Ostracode marine şi salmastricole). Fauna R.S. R. Crustacea (Ostracoda), IV(10), pp. 1–164.

Catianis, I., Secrieru, D., Pojar, I., Grosu, D., Scrieciu, A., Pavel, A.B., Vasiliu, D., 2018. Water quality, sediment characteristics and benthic status of the Razim-Sinoie lagoon system, Romania. Open Geosci. 10, 12–33.

Catianis, I., Constantinescu, A.M., Grosu, D., Rotaru, S., Briceag, A., 2020. Analysis of the physical and chemical parameters to characterize water quality condition in Lake Matita, Danube Delta, Romania. Int. Multidiscip. Sci. GeoConf. 20 (3.1), 19–26.

Chaumillon, E., Bertin, X., Fortunato, A.B., Bajo, M., Schneider, J.L., Dezileau, L., Walsh, J.P., Michelot, A., Chauveau, E., Créach, A., Hénaff, A., 2017. Storm-induced marine flooding: lessons from a multidisciplinary approach. Earth Sci. Rev. 165, 151–184.

Conea, A., 1970. Quaternary Deposits of Dobrudja. Academia Publishing House, Bucharest (in Romanian).

Culicov, O.A., Trtić-Petrović, T., Nekhoroshkov, P.S., Zinicovscaia, I., Duliu, O.G., 2022. On the geochemistry of the Danube river sediments (Serbian sector). Int. J. Environ. Res. Public Health 19 (19), 12879.

Dan, S., Stive, M.J., Walstra, D.J.R., Panin, N., 2009. Wave climate, coastal sediment budget and shoreline changes for the Danube Delta. Mar. Geol. 262 (1–4), 39–49.

Debenay, J.P., Geslin, E., Eichler, B.B., Duleba, W., Sylvestre, F., Eichler, P., 2001. Foraminiferal assemblages in a hypersaline lagoon, Araruama (RJ) Brazil. J. Foraminiferal Res. 31 (2), 133–151.

Degeai, J.P., Devillers, B., Dezileau, L., Oueslati, H., Bony, G., 2015. Major storm periods and climate forcing in the Western Mediterranean during the late Holocene. Quat. Sci. Rev. 129, 37–56.

Dimitriu, R.G., 2012. Geodynamic and hydro-geological constraints regarding the extension of the prospective archaeo-cultural area within the northern Romanian coastal zone. Quat. Int. 261, 32–42.

Dinescu, L., Steinnes, E., Duliu, O., Ciortea, C., Sjobakk, T., Dumitriu, D., Gugiu, M., Haralambie, M., 2004. Distribution of some major and trace elements in Danube Delta lacustrine sediments and soil. J. Radioanal. Nucl. Chem. 262 (2), 345–354.

Duck, R.W., Da Silva, J.F., 2012. Coastal lagoons and their evolution: A hydromorphological perspective. Estuar. Coast. Shelf Sci. 110, 2–14.

Folk, R.L., Ward, W.C., 1957. Brazos River bar [Texas]; a study in the significance of grain size parameters. J. Sediment. Res. 27 (1), 3–26.

Frenzel, P., Boomer, I., 2005. The use of ostracods from marginal marine, brackish waters as bioindicators of modern and quaternary environmental change. Palaeogeogr. Palaeoclimatol. Palaeoecol. 225 (1–4), 68–92.

Giaime, M., Marriner, N., Morhange, C., 2019. Evolution of ancient harbours in deltaic contexts: A geoarchaeological typology. Earth Sci. Rev. 191, 141–167.

Giosan, l., Donnelly, J., Vespremeanu, E., Constantinescu, S., Filip, F., Ovejanu, I., Vespremeanu, S.A., Duller, G.A.T., 2006. Young Danube delta documents stable Black Sea level since the middle Holocene: Morphodynamic, paleogeographic and archeological implications. Geology 34 (9), 757–760.

Grossu, A.V., 1955. Fauna R.P.R. Vol. III Fasc. 1 Mollusca. Gastropoda Pulmonata, III.1. Ed. Academiei Republicii Populare Romane (518 pp).

Grossu, A.V., 1956. Fauna R.P.R. Vol. III Fasc. 2 Mollusca. Gastropoda Prosobranchia, III.2. Ed. Academiei Republicii Populare Romane (220 pp).

Hayward, B.W., 2014. "Monospecific" and near-monospecific benthic foraminiferal faunas, New Zealand. J. Foraminiferal Res. 44 (3), 300–315.

Heaton, T.J., Köhler, P., Butzin, M., Bard, E., Reimer, R.W., Austin, W.E., Ramsey, C.B., Grootes, P.M., Hughen, K.A., Kromer, B., Reimer, P.J., 2020. Marine20—the marine radiocarbon age calibration curve (0–55,000 cal BP). Radiocarbon 62 (4), 779–820.

Heiri, O., Lotter, A.F., Lemcke, G., 2001. Loss on ignition as a method for estimating organic and carbonate content in sediments: reproducibility and comparability of results. J. Paleolimnol. 25, 101–110.

Holmes, J.A., De Deckker, P., 2012. The chemical composition of ostracod shells: Applications in quaternary palaeoclimatology. In: Developments in Quaternary Sciences, vol. 17. Elsevier, pp. 131–143.

Întorsureanu, I., Colios, E., Grabari, G., Popescu, G., Şerbănescu, A., 1989. Petrologia asociaţiei granitelor alkaline din masivele Iacobdeal şi Piatra Roşie (Dobrogea de nord). D.S. Inst. Geol. Geofiz. 74 (I), 67–86.

Kaminski, M.A., Aksu, A., Box, M., Hiscott, R.N., Filipescu, S., Al-Salameen, M., 2002. Late glacial to Holocene benthic foraminifera in the Marmara sea: implications for Black Sea–Mediterranean sea connections following the last deglaciation. Mar. Geol. 190 (1–2), 165–202.

Marco-Barba, J., Holmes, J.A., Mesquita-Joanes, F., Miracle, M.R., 2013. The influence of climate and sea-level change on the Holocene evolution of a Mediterranean coastal lagoon: evidence from ostracod palaeoecology and geochemistry. Geobios 46 (5), 409–421.

Mazzini, I., Aiello, G., Frenzel, P., Pint, A., 2022. Marine and marginal marine Ostracoda as proxies in geoarchaeology. Mar. Micropaleontol. 174, 102054.

Meisch, C., 2000. Freshwater Ostracoda of Western and Central Europe, 8 (3). Spektrum Academischer, Heidelberg, p. 522.

Mischke, S., Schudack, U., Bertrand, S., Leroy, S.A., 2012. Ostracods from a Marmara Sea lagoon (Turkey) as tsunami indicators. Quat. Int. 261, 156–161.

Morhange, C., Marriner, N., Bony, G., Flaux, C., Giaime, M., Kouka, M., 2016. Geoarchaeology of ancient harbours in lagoonal contexts: an introduction. In: Franconi, T. (Ed.), Fluvial Landscapes in the Roman World, pp. 97–110 (Journal of Roman archaeology, supplementary series 104. Portsmouth, Rhode Island).

Musat, A., 2017. Early roman finds from acic suat (Caraburun, Baia, Tulcea county). Peuce (Serie Nouă)-Studii şi cercetari de istorie şi arheologie 15 (15), 279–294.

Opreanu, P.A., 2008. Ostracode relicte Ponto-Caspice in sectorul Romanesc al Marii Negre. GeoEcoMarina 14, 57–62.

Ortega, P., Lehner, F., Swingedouw, D., Masson-Delmotte, V., Raible, C.C., Casado, M., Yiou, P., 2015. A model-tested North Atlantic Oscillation reconstruction for the past millennium. Nature 523 (7558), 71–86.

Panin, N., 1989. Danube Delta. Genesis, evolution and sedimentology. Revue Roumaine de Geographie, Geologie, Geophysique 33, 25–36.

Preoteasa, L., Vespremeanu-Stroe, A., Panaiotu, C., Rotaru, S., Ţuţuianu, L., Sava, T., Birzescu, I., Dimofte, D., Sava, G., Mirea, D.A., Ailincăi, S., 2019. Neolithic to modern period palaeogeographic transformations in southern Danube delta and their impact on human settlements in the Enisala-Babadag region. Quat. Int. 504, 139–152.

Sabatier, P., Dezileau, L., Barbier, M., Raynal, O., Lofi, J., Briqueu, L., Condomines, M., Bouchette, F., Certain, R., Van Grafenstein, U., Jorda, C., 2010. Late-Holocene evolution of a coastal lagoon in the Gulf of lions (south of France). Bull. Soc. Geol. Fr. 181 (1), 27–36.

Sabatier, P., Dezileau, L., Colin, C., Briqueu, L., Bouchette, F., Martinez, P., Siani, G., Raynal, O., Von Grafenstein, U., 2012. 7000 years of paleostorm activity in the NW Mediterranean Sea in response to Holocene climate events. Quat. Res. 77 (1), 1–11.

Sabatier, P., Moernaut, J., Bertrand, S., Van Daele, M., Kremer, K., Chaumillon, E., Arnaud, F., 2022. A review of event deposits in Lake sediments. Quaternary 5, 34.

Săndulescu, M., 1984. Geotectonica României. Editura Tehnică (335 pp).

Scrieciu, A., Rotaru, S., Alexandrescu, B., Catianis, I., Nanu, F., Marchal, R., Pagano, A., Giordano, R., 2023a. Reducing water related risks in the lower Danube through nature based solution design: A stakeholder participatory process. In: Greening Water Risks: Natural Assurance Schemes. Springer International Publishing, Cham, pp. 171–199.

Scrieciu, A., Rotaru, S., Lupascu, N., Pavel, B., Toma, A., Bogos, F., 2023b. Monitorizarea parametrilor hidromorfologici şi de calitate a apei în sectoarele reprezentative selectate de pe cursul inferior al Dunării. PN 23300303 Scientific Report, Bucharest.

Seghedi, A., 2012. Palaeozoic formations from Dobrogea and pre-Dobrogea – an overview. Turk. J. Earth Sci. 669721, 21/2012.

Seghedi, I., Szakacs, A., Udrescu, C., Grabari, G., Stoian, M., Tănăsescu, A., Vlad, C., 1992. Major and trace element geochemistry of rhyolites from northern Dobrogea; petrogenetic implications. Rom. J. Petrol. 75, 17–38.

Siani, G., Paterne, M., Arnold, M., Bard, E., Métivier, B., Tisnerat, N., Bassinot, F., 2000. Radiocarbon reservoir ages in the Mediterranean Sea and in Black Sea. Radiocarbon 42 (2), 271–280.

Sorrel, P., Debret, M., Billeaud, I., Jaccard, S.L., McManus, J.F., Tessier, B., 2012. Persistent non-solar forcing of Holocene stormdynamics in coastal sedimentary archives. Nat. Geosci. 5, 892–896.

Stoica, M., Lazar, I., Krijgsman, W., Vasiliev, I., Jipa, D.C., Floroiu, A., 2013. Palaeoenvironmental evolution of the east Carpathian foredeep during the late Miocene - early Pliocene (Dacian Basin; Romania). Glob. Planet. Chang. 103, 135–148.

Tang, D., Chen, M., Huang, X., Zhang, G., Zeng, L., Zhang, G., Wu, S., Wang, Y., 2023. SRplot: A free online platform for data visualization and graphing. PLoS One 18 (11), e0294236.

Tugulan, L.C., Duliu, O.G., Bojar, A.V., Dumitras, D., Zinicovskaia, I., Culicov, O.A., Frontasyeva, M.V., 2016. On the geochemistry of the late quaternary loess deposits of Dobrogea (Romania). Quat. Int. 399, 100–110.

Vadineanu, A., Cristofor, S., Ignat, G., Romanca, G., Ciubuc, C., Florescu, C., 1997. Changes and opportunities for integrated management of the Razim-Sinoe lagoon system. Int. J. Salt Lake Res. 6, 135–144.

Van de Velde, S., Jorissen, E.L., Neubauer, T.A., Radan, S., Pavel, A.B., Stoica, M., Van Baak, C.G.C., Gandara, A.M., Popa, L., Stigter, H., Abels, H.A., Krijgsman, W., Wesselingh, F.P., 2019. A conservation palaeobiological approach to assess faunal response of threatened biota under natural and anthropogenic environmental change. Biogeosciences 16, 2423–2442.

Vespremeanu-Stroe, A., 2004. Transportul de sedimente în lungul tarmului si regimul valurilor pe coasta Deltei Dunarii. Studii si Cercetari de Oceanografie Costiera 1, 67–82.
Vespremeanu-Stroe, A., Tătui, F., 2011. North-Atlantic oscillation signature on coastal dynamics and climate variability of the Romanian Black Sea coast. Carpathian J. Earth Environ. Sci. 6 (1), 308–316.
Vespremeanu-Stroe, A., Constantinescu, Ş., Tătui, F., Giosan, L., 2007. Multi-decadal evolution and North Atlantic oscillation influences on the dynamics of the Danube Delta shoreline. J. Coast. Res. 50 (sp1), 157–162.
Vespremeanu-Stroe, A., Preoteasa, L., Hanganu, D., Brown, T., Birzescu, I., Toms, P., Timar-Gabor, A., 2013. The impact of the late Holocene coastal changes on the rise and decay of the ancient city of Histria (southern Danube delta). Quat. Int. 293, 245–256.
Vespremeanu-Stroe, A., Preoteasa, L., Zăinescu, F., Rotaru, S., Croitoru, L., Timar-Gabor, A., 2016. Formation of Danube delta beach ridge plains and signatures in morphology. Quat. Int. 415, 268–285.
Vespremeanu-Stroe, A., Zăinescu, F., Preoteasa, L., Tătui, F., Rotaru, S., Morhange, Ch., Stoica, M., Hanganu, J., Timar-Gabor, A., Cârdan, I., Piotrowska, N., 2017. Holocene evolution of the Danube delta: an integral reconstruction and a revised chronology. Mar. Geol. 388, 38–61.
Zaharia, L., Pisota, I., 2003. Apele dobrogei. In: Annals of the University of Bucharest–Geography Series, 52. University of Bucharest, Faculty of Geography, Bucharest, pp. 107–143.
Zăinescu, F.I., Tătui, F., Valchev, N.N., Vespremeanu-Stroe, A., 2017. Storm climate on the Danube delta coast: evidence of recent storminess change and links with large-scale teleconnection patterns. Nat. Hazards 87 (2), 599–621.
Zăinescu, F.I., Vespremeanu-Stroe, A., Tătui, F., 2019. The formation and closure of the big breach of Sacalin spit associated with extreme shoreline retreat and shoreface erosion. Earth Surf. Process. Landf. 44 (11), 2268–2284.
Zenkovich, V.P., 1956. Zagadka Dunaiskoi Deltî. Priroda 45 (3), 86–90.